High-frequency carbonate cycles and stacking patterns: Interplay of orbital forcing and subsidence on Lower Jurassic rift platforms, High Atlas, Morocco

Paul D. Crevello[1]

Abstract The stratigraphy of carbonate cycles and cycle-stacking patterns in Lower Jurassic shallow-water platforms from the High Atlas rift are related to base-level changes driven by orbital forcing and subsidence. Multifold platform stratigraphic hierarchy, originally recognized from field observations, yields cycle ratios approximating 20:5:1 with time-thickness (Fischer plots) and time-series analyses. The cycle ratios are similar to orbital cycles of long and short eccentricity and precession. A depositional sequence model for cycle-stacking patterns, which is governed by a threefold superimposed sea-level curve that yields a 20:5:1 cycle ratio, is compared with the stratigraphic field data. Divergence of Jurassic cycle distribution and stacking patterns from the ideal model suggest that subsidence and variation in long-term eccentricity controlled the development of progradational, aggradational, or retrogradational stacking patterns and thus dictated the resulting distribution of systems tracts within depositional sequences. The lithofacies character and cycle symmetry of individual carbonate cycles are controlled by local environmental conditions in addition to eustasy and subsidence. Cycles are considered the fundamental stratigraphic element constructing the platforms. However, the contribution of complete cycles to the overall stratigraphic record of the platform is varied. Outer-platform cyclic strata make up nearly 75% of the stratigraphic interval. In contrast, platform-margin or inner-platform strata contain less than 50% complete cycles. The balance at the outer platform between subsidence and the interplay of *high-frequency* and *low-amplitude* sea-level fluctuations of 1–5 m (3–16 ft) accounts for the higher percentage of cycles in shallow-water settings. Inner-platform strata were limited by creation of accommodation space, and platform-margin strata were too deep on the distally steepened margin to be influenced by every base-level shift that affected shallow-water sedimentation. Only infrequently did high-amplitude sea-level falls, of the order of 30 m (100 ft), expose sediments at the platform margin.

Shallow-water carbonate platforms provide a sensitive gauge for recording high-frequency sea-level changes at the scale of shallowing-upward cycles (James, 1984; Kendall and Schlager, 1981; Hardie and Shinn, 1986). The stratigraphic signatures encoded in platform cycle-stacking patterns, however, only recently have been investigated for their long-term record of eustasy and subsidence (Fischer, 1964; Schwarzacher, 1987; Goldhammer et al., 1987; Read and Goldhammer, 1988; Bond et al., 1989; Crevello, 1990b). Schwarzacher's analyses of stratification cycles provide some of the earliest demonstrations of cycle periodicity and quantitative stratigraphic modeling (Schwarzacher, 1964, 1975, 1987). Fischer (1964) used thickness-time plots of Löfer cyclothems to interpret tectonic control on platform stratigraphy; more recently, these plots have been applied as long-term eustatic (Read and Goldhammer, 1988) or accommodation curves (Dunn et al., 1991). Spectral methods are now frequently applied to derive cycle periodicity and to assign duration to deposition of strata (Weedon, 1986; Schwarzacher, 1987; Read and Goldhammer, 1988; Kominz and Bond, 1990, this volume); the advantages and limitations of these methods are presented by the various researchers. Foremost, the field and numerical studies on cycle-stacking patterns demonstrate the need to evaluate high-quality stratigraphic data sets with time-thickness and time-series analyses of cycle periodicity to test rigorously the controls on depositional sequences and to constrain stratigraphic models.

In this article I investigate high-frequency cycles and stacking patterns from two structurally separate but coeval Jurassic platforms in the Central and Eastern High Atlas rift (Sinemurian–Pliensbachian age). High rates of subsidence associated with rifting were crucial for preserving an exceptional vertical record of platform stratigraphy. The superb data set demonstrates the development and variability of shallowing-upward cycles and stacking patterns across a rift platform. In addition, the eustatic and subsidence controls on the hierarchy of stratigraphic packaging are presented for the high-frequency carbonate sequences (10^4–10^5 years), and contrasted with a high-frequency low-amplitude depositional sequence model.

Geologic setting

The High Atlas mountains occupy a continental shear zone that borders the northwest margin of Africa (fig. 1). The shear zone is separated from the relatively stable Saharan shield by the South Atlas fault system, which has been a prominent structural boundary since the Hercynian (late Paleozoic)

1. Petroleum Technology Center, Marathon Oil Company, PO Box 269, Littleton, CO 80160.

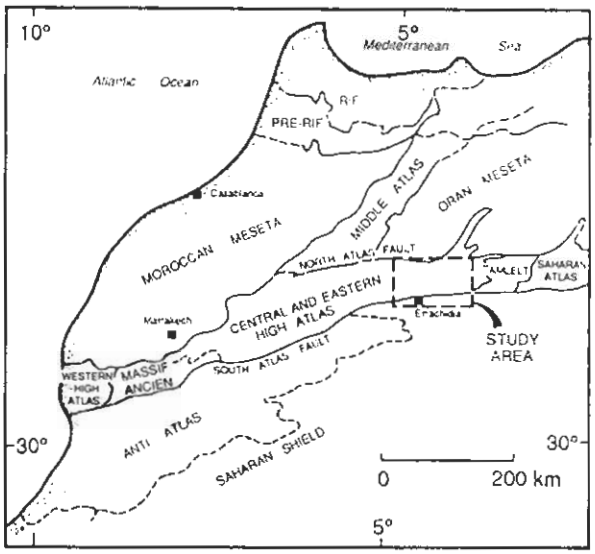

Figure 1. Regional setting and major structural provinces of Morocco.

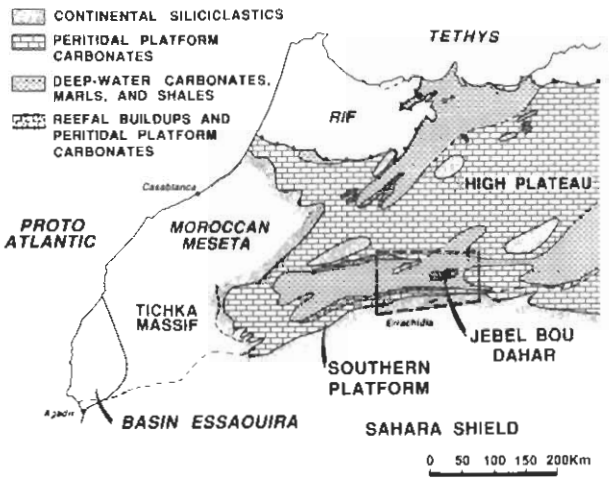

Figure 2. Middle Liassic (Pliensbachian) paleogeographic reconstruction of Morocco modified after Dresnay (1979) and Septfontaine (1986). East-west-trending deep-water deposits approximate the location of major rift subsidence. See fig. 3 for details of inset map.

(Mattauer et al., 1972). The Atlas mountains have a polyphase orogenic history that includes Hercynian deformation, Mesozoic wrench-rift tectonics, and Alpine inversion. Rifting began in the Triassic and accelerated during the Liassic (Early Jurassic) in response to the opening of the North Atlantic and the separation of Europe and Africa. Stets and Wurster (1982) proposed that during the Jurassic the actively subsiding rifts or shear zones of the Middle and High Atlas were separated by structurally stable mesetas (fig. 1).

The rift zones were marine seaways during the middle Liassic (Dresnay, 1979; Crevello, 1990b) (figs. 2 and 3). The narrow seaways terminated with shorelines near the structural high of the Tichka massif, along the Moroccan meseta, and along the southern border with the Sahara. The seaways approximate the region of main subsidence within the rifts, which were filled with deep-water limestone and marl, whereas the margins developed shoal-water carbonates.

Depositional facies and synrift depositional models incorporate oblique extension to strike-slip compression for platform and basin strata in the High Atlas (Lee and Burgess, 1978; Jenny et al., 1981; Monbaron, 1981; Crevello et al., 1987; Crevello, 1988, 1990b; Jossen, 1987). Two stages of platform development are recognized along the margin of the rift (Dresnay, 1979) (fig. 4): (1) lower to middle Liassic (Sinemurian to Domerian) lower platform complex and (2) upper Liassic to lower Dogger (Aalenian to Bajocian–Bathonian?) upper platform complex (Crevello, 1990b). The lower platform complex was drowned in the Toarcian, and, as a consequence, the southern platform was blanketed by Toarcian and Aalenian ammonite-bearing marine shales (Crevello, 1990b). Here, I focus on the lower platform complex of the southern Saharan platform and the axial-rift platform of Jebel Bou Dahar. Strata of the southern platform are only moderately structurally disrupted and are essentially horizontal and exposed in incised river valleys of hinged thrust plateaus. The exhumed axial-rift platform, Jebel Bou Dahar, is preserved with undeformed platform to basin strata relationships (Agard and Dresnay, 1965; Crevello, 1988, 1990b).

Small-scale carbonate cycles

Small-scale carbonate cycles are considered here as the fundamental stratigraphic element of platforms [see Wanless (this volume)]. The depositional units represent vertical facies successions of marine carbonate sediments, cyclic or noncyclic, which are bounded by subaerial exposure surfaces or marine flooding surfaces. When a repetitive facies succession is defined, the depositional unit is distinguished as a cycle. Shallowing-upward cycles (James, 1984) are the dominant type of platform cycle and are equivalent to parasequences (Sarg, 1988; Van Wagoner et al., 1988). Cycles typically have a duration of 10^4–10^5 years [see Goldhammer et al. (this volume)].

Carbonate shallowing-upward cycles are the dominant depositional units of the High Atlas platform strata. Four types of cycles and their distribution across the platform have been documented by field mapping (figs. 5 and 6): (1) skeletal grainstone cycles, (2) ooid grainstone cycles, (3) skeletal-bivalve-oncolite packstone-wackestone cycles, and (4) peloid-laminate wackestone-packstone cycles. Lithofacies of these cycles are commonly arranged in asymmetric cycles made up of repeated lithofacies such as patterns of a–b–c–a–b–c (James, 1984) (fig. 5). Outer-platform cycles also develop with symmetric arrangements, such as c–b–a–b–c

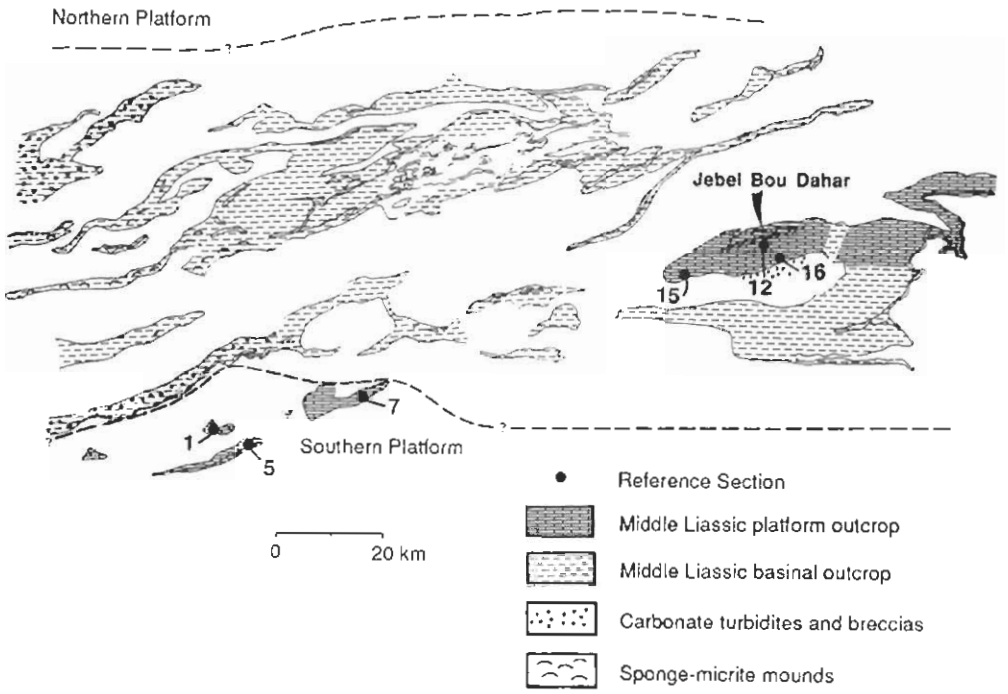

Figure 3. Reconstruction and outcrop distribution of middle and upper Sinemurian–Domerian platforms and basins. Measured sections are discussed in the text. Sections 1, 5, and 7 are located in the southern platform; sections 12, 15, and 16 are located in the exhumed axial-rift platform of Jebel Bou Dahar.

[see also Schwarzacher (1987)]. In addition, incomplete cycles, which are characterized by top-truncated caps (e.g., a–b lithofacies), and noncyclic strata of a, b, or c lithofacies are common depositional units of the platform. Characteristics, variations, and distribution of the cyclic and noncyclic depositional units are presented in the next section.

Skeletal grainstone cycles

Distribution and lithofacies Skeletal grainstone cycles are common in outer-platform and platform-margin strata. This cycle type consists of subtidal, biotically diverse skeletal lithofacies at the base and mixed skeletal-oolite lithofacies in the upper parts of the shallow subtidal to intertidal cap (figs. 5–7). The skeletal grainstone portion of the cycle consists of medium- to thick-bedded [0.5–1.0 m (1.6–3 ft)], bioturbated limestones of packstone to boundstone-framestone textures that are rich in corals, bivalves, and calcareous algae. The skeletal lithofacies grade upward into medium- to thin-bedded [0.2–0.5 m (0.7–1.6 ft)], burrowed to cross-stratified, mixed skeletal-oolite lithofacies, which, in turn, grade upward into capping beds of keystone fenestral, parallel- to cross-stratified oolite lithofacies. The base of each skeletal cycle is separated from the underlying cycle by either a subaerial exposure surface or a marine flooding surface. The tops of cycles exposed to subaerial weathering are

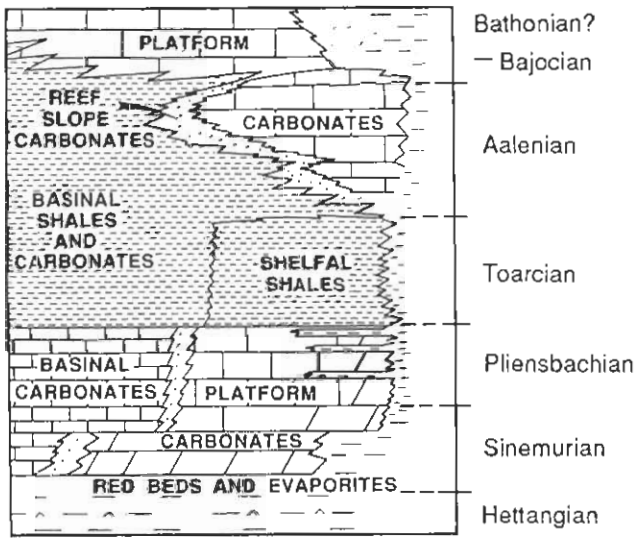

Figure 4. Jurassic stratigraphic column of the southern platform, Central and Eastern High Atlas.

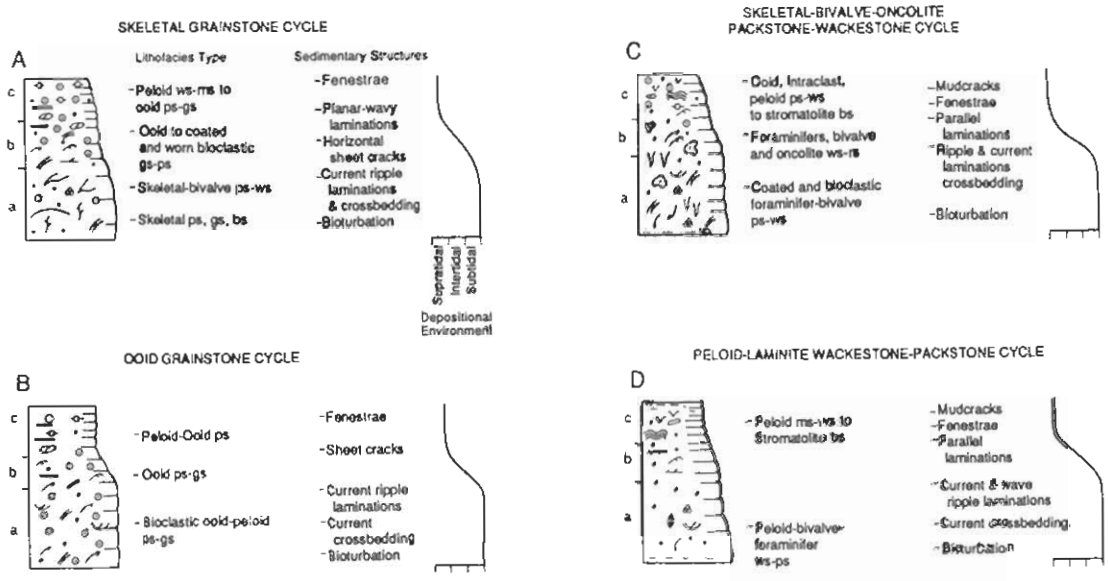

Figure 5. Types of peritidal shallowing-upward cycles. (A) Skeletal grainstone cycle. (B) Ooid grainstone cycle. (C) Skeletal-bivalve-oncolite packstone-wackestone cycle. (D) Peloid-laminite wackestone-packstone cycle. ms, mudstone; ws, wackestone; ps, packstone; gs, grainstone; rs, rudstone; bs, boundstone; fs, floatstone.

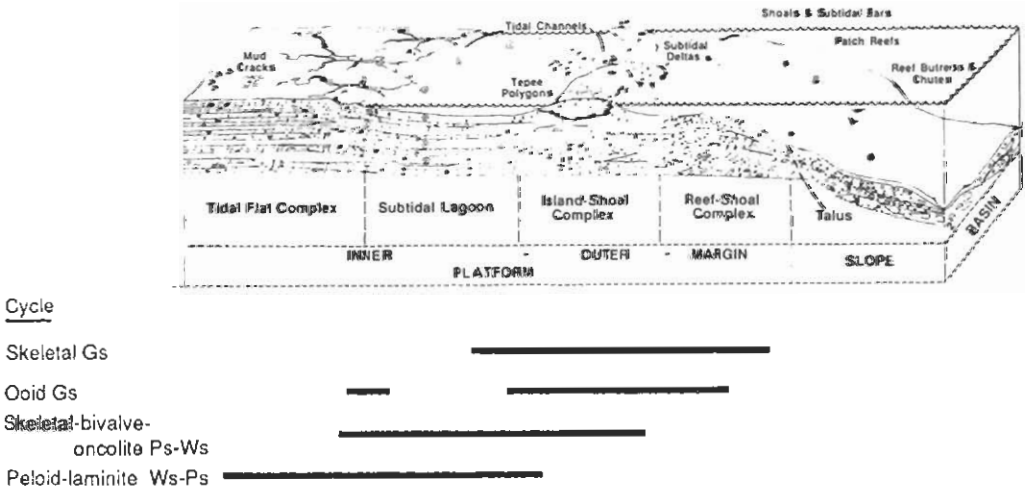

Figure 6. Schematic cross section of middle Liassic platform facies belts illustrating distribution of shallowing-upward peritidal cycles. Facies relationships of the inner-platform lagoon and tidal flat are modified from Septfontaine (1986); outer-platform to basin facies relationships are from Crevello (1990b). See fig. 5 for definition of abbreviations.

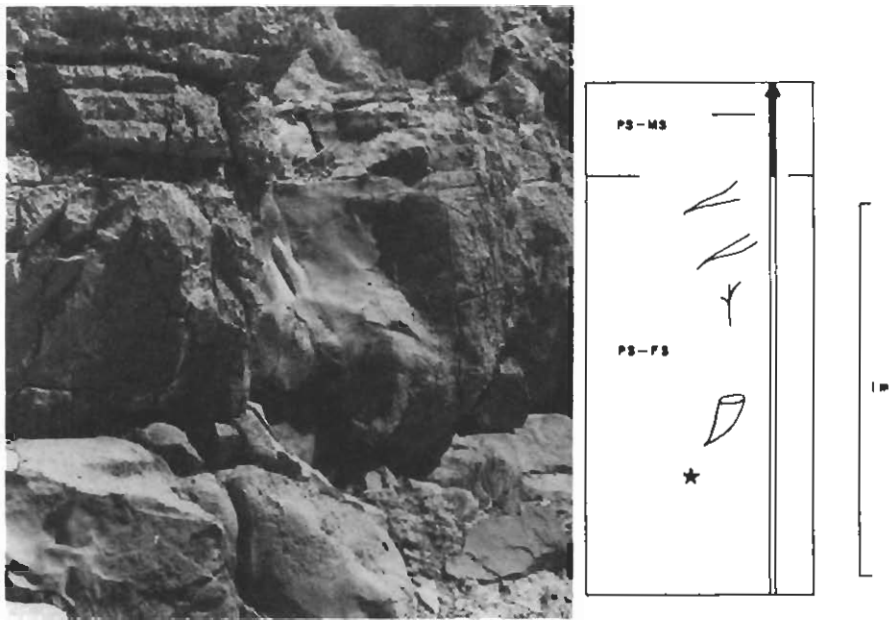

Figure 7. Massively bedded, skeletal grainstone cycle with basal bivalve-coral floatstone to packstone capped by horizontal sheet cracks and very thin bedded, laminated, ooid-peloid packstone to mudstone. Drawing illustrates the bottom and the top of the cycle: open double line marks the subtidal portion of the cycle; solid line marks the intertidal and supratidal cap. See fig. 5 for definition of abbreviations.

microkarsted and are composed of autoclastic breccias containing micrite-filled fossil molds or are capped by a red argillaceous crust or thin red shale.

Cycle variation Skeletal grainstone cycles also occur as incomplete top-truncated asymmetric cycles that consist of erosionally truncated, subtidal, skeletal or skeletal-oolite lithofacies that are capped by subaerial diagenetic crusts (fig. 8). These cycles lack shallowing-upward intertidal and supratidal capping lithofacies. Top-truncated cycles result from subaerial exposure of subtidal lithofacies, with only minor erosion and calichification associated with karstification. Similar cycles were described by Fischer (1964) as Triassic Löfer cycles.

Skeletal grainstone cycles also occur as symmetric cycles. The basal lithofacies of symmetric cycles are thin- to thick-bedded [0.2–1.0 m (0.7–3.0 ft)], fenestral and parallel- to crossbedded, skeletal or oolite lithofacies that grade upward into subtidal, burrowed, skeletal-oolite lithofacies. The symmetric succession of lithofacies records an initial deepening, or base-level rise, into subtidal lithofacies and then a gradual shallowing-upward to a subaerial exposure cap or flooding surface.

Ooid grainstone cycles

Distribution and lithofacies Ooid grainstone cycles occur primarily in outer-platform strata of island and subtidal shoal complexes. Ooid grainstone cycles are dominated by grain-rich ooid lithofacies with subordinate skeletal and peloidal lithofacies. Locally, isolated in situ growths of corals, bivalves, or stromatolites occur in the bases of cycles (fig. 9). The thin- to medium-bedded [0.2–0.5 m (0.7–1.6 ft)] ooid grainstones are bioturbated, parallel laminated, or crossbedded, with the thickness of bedsets decreasing upward in the cycle. Thinly bedded [0.2 m (0.7 ft)], fenestral, parallel- and cross-laminated ooid or peloid grainstones and packstones cap the cycle.

Ooid grainstone cycles that were exposed to subaerial weathering are capped by red argillaceous crusts or thin red shales. Synsedimentary isopachous cements are pervasive in ooid grainstones interpreted as subtidal and intertidal deposits, and locally incipient horizontal sheet cracks and tepee bedding are developed in capping strata of intertidal and supratidal peloid-ooid grainstone-packstones.

Cycle variation Symmetric cycles of ooid grainstones, including incipient tepee bedding, occur locally in outer-platform strata of Jebel Bou Dahar, where they developed with island-shoal oolite bar systems. The bases of symmetric cycles consist of low-angle, parallel-laminated and fenestral, ooid-peloid grainstone-packstone or of stromatolitic ooid-peloid grainstones that grade into a burrowed subtidal portion of the ooid grainstone cycle. The basal lithofacies in symmetric cycles are typically thin, less than 0.5 m (<1.6 ft), relative to capping lithofacies, which are 1.0–2.5 m (3.3–8.2 ft) thick. Consequently, the shallowing-upward portion of symmetric cycles is thicker.

Figure 8. Top-truncated subtidal limestone of skeletal bivalve-coral floatstone-packstone capped by a subaerial unconformity (arrow), which is overlain by crossbedded ooid-peloid grainstones. Section is from the transgressive systems tract that caps the southern platform. Scale bar is 10 cm.

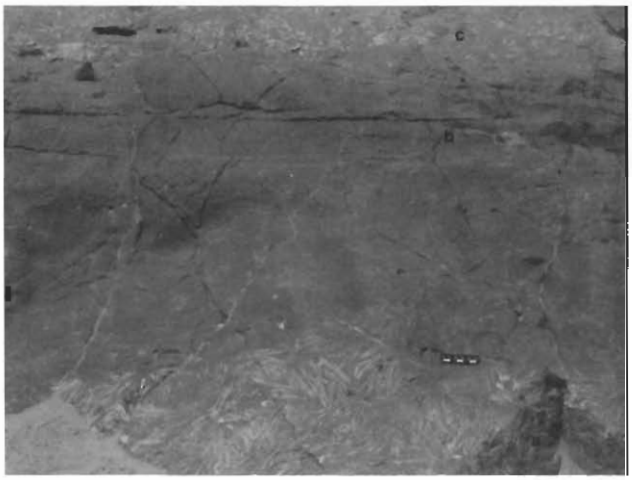

Figure 9. Base of shallowing-upward ooid grainstone cycle containing both wave-reworked and in situ thin-walled chrondrodontid bivalves in ooid packstone-grainstone. The cycle grades upward into low-angle stratified, fenestral ooid-peloid grainstone. Scale bar is 10 cm.

Pisoid-tepee caps of ooid grainstone cycles represent depositional and diagenetic modifications of the cycle. The ooid and pisoid lithofacies were deposited in shallow intertidal to supratidal settings and were disrupted by sheet cracks and tepee structures (Burri et al., 1973; Kendall and Warren, 1987). The tepee structures preserve meteoric vadose fabrics of geopetal micrite-infilled fossil molds and meniscus cements. Syndepositional features include isopachous, radial-fibrous cements of phreatic marine origin, marine carbonate sediment fillings of upturned tepee cracks, and beveled tepee surfaces overlain by marine sediment.

Symmetric cycles with tepee-bedded basal lithofacies occur in island-shoal complexes along the platform margin of Jebel Bou Dahar. Tepee-bedded ooid-pisoid rudstones grade upward into asymmetric ooid grainstone cycles, which, in turn, are capped by tepee-bedded pisoid lithofacies. The basal lithofacies of symmetric ooid cycles are thin relative to the shallowing-upward portion of these cycles, which is similar to symmetric skeletal grainstone cycles.

Skeletal-bivalve-oncolite packstone-wackestone cycles

Distribution and lithofacies The lithofacies assemblage of the packstone-wackestone cycles reflects deposition in areas transitional to the inner platform that were protected from high-energy conditions, such as areas in the lee of islands and shoals (figs. 5, 6, and 10). The skeletal-bivalve-oncolite cycles consist of 1–2-m-thick (3–7-ft-thick), medium- to thick-bedded [0.5–1.0 m (1.6–3.3 ft)], subtidal mud-rich lithofacies composed of lithiotid bivalves or oncolites in skeletal and coated-grain lithofacies (fig. 10). The subtidal lithofacies grade upward into thin-bedded, moderately fossiliferous, fenestral peloid-ooid packstone and grainstone lithofacies and locally into stromatolite boundstones. Upper intertidal and supratidal lithofacies are thin-bedded [0.2 m (0.7 ft)] to laminated, alternating mud-rich and grain-rich strata. Intraclasts include grapestone aggregates, mud chips, and, less common, oolite clasts. Polygonal mudcracks and syneresis cracks developed in intertidal and supratidal strata. Septfontaine (1986) contrasted the autochthonous microfauna of the lower subtidal

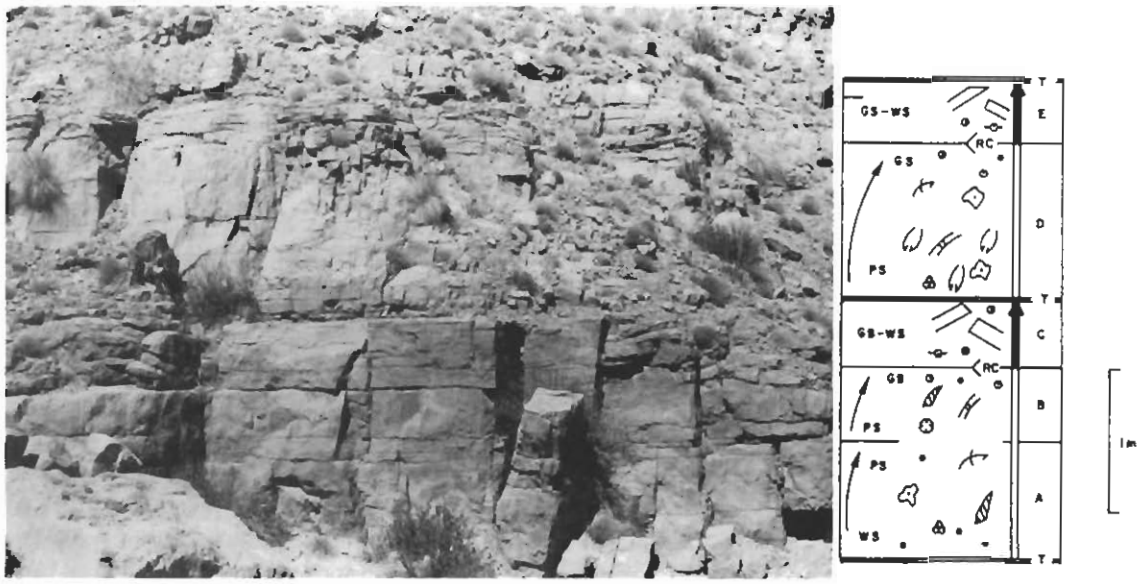

Figure 10. Shallowing-upward limestones of skeletal-bivalve-oncolite cycles with wackestones capped by fenestral, tepee-bedded peloid-ooid lithofacies. Two complete cycles are present; the lower cycle grades from a subtidal (open double line) base of bivalve-oncolite lithofacies (A) to a lower to upper intertidal (shaded line) bioclast packstone to ooid grainstone lithofacies disrupted by tepee bedding. The subaerial crusts (RC) cap the upper intertidal lithofacies, which is beneath the tepee-bedded interval. The tops of the cycles (T) represent exposure surfaces, bedding discontinuities, and transgressive surfaces. Lithofacies are distinctly different across this surface, which reflects base-level control on cycle development. See fig. 5 for definition of abbreviations.

portion of this cycle with the allochthonous microfauna displaced into the supratidal deposits by storm processes.

Basal transgressive lags locally contain mud-clast pebbles, skeletal hash, and silt or clay. Cycle caps are typically marked by subaerial exposure surfaces that are microkarsted and characterized by autoclastic breccias with fossil molds filled by red-yellow micrite. The caps are red-yellow argillaceous crusts or thin red shales.

Cycle variation Skeletal-bivalve-oncolite cycles are abundant in protected outer- to inner-platform facies belts of Jebel Bou Dahar and the southern Saharan platform, where they occur only as complete asymmetric cycles (i.e., a–b–c cycles) or top-truncated (a–b) asymmetric cycles (fig. 11). Top-truncated cycles lack the capping fenestral, peloid packstone and grainstone lithofacies. Instead, subtidal and intertidal lithofacies are capped by subaerial autoclastic breccias and red crusts. Septfontaine (1986) noted similar variations in cycles from the western margin of the High Atlas trough, which developed top-truncated (c–b–a–b) symmetric cycles. These cycles consist of basal, supratidal, fenestral stromatolites that grade upward into burrowed oncolite-skeletal wackestones. The subtidal skeletal wackestone lithofacies are capped by diagenetic crusts and thus are top-truncated cycles.

Peloid-laminate wackestone-packstone cycles

Distribution and lithofacies Peloid-laminate cycles developed with limited skeletal diversity in mud-rich lithofacies (figs. 5, 6, and 12). Nodular thin-bedded to medium-bedded [0.2–0.5 m (0.7–1.6 ft)] subtidal lithofacies consist mostly of peloids, crustacean pellets, ostracodes, bivalves, gastropods, oncolites, and, less common, benthic foraminifers and calcareous algae. The subtidal lithofacies grade upward into thin-bedded [0.2 m (0.7 ft)] to laminated, fenestral bioclastic peloid and stromatolite (crinkly and domal stromatolites) upper intertidal and supratidal lithofacies, which are characterized by mudcracks, syneresis shrinkage cracks, soft-pellet ripples, and flat-pebble mud chips. Noncyclic strata interbedded with the cycles consist of reddish-beige argillaceous dolomudstones with deep [5–8 cm (2–3 in.)] polygonal mudcracks, irregular wavy to nodular bedding associated with domal stromatolites, shallow [10–20 cm (4–8 in.)] cut-and-fill structures, and locally minor evaporites.

Basal transgressive lag deposits developed locally with pebbles of mudstone, silt, or clay. The tops of the cycles are marked by diagenetic surfaces of microkarst composed of autoclastic breccias or capped by red to yellow argillaceous crusts or thin red shales.

Figure 11. Top-truncated skeletal bivalve packstone (a) capped by subaerial unconformity (dashed line) and overlain by laminated, fenestral, peloid dolopackstone (b). Karst with dissolution channels caps the limestone. The section is from the top of the retrogradational sequence 5 shown in fig. 20. This surface is a type 2 or type 3 unconformity. The total thickness of the amalgamated beds is 1.5 m (5.0 ft).

Cycle variation Peloid-laminate cycles are common inner-platform asymmetric cycles of the southern platform, where they are dolomite, and in the interior of the Jebel Bou Dahar platform, where they are mainly limestone interbedded with alluvial-plain silty shale. Complete symmetric cycles were not observed in inner-platform facies belts. However, incomplete cycles, such as top-truncated cycles, and noncyclic depositional sequences were common in the inner platform. Top-truncated cycles consist of sparsely fossiliferous peloid wackestone-packstones capped by autoclastic breccias. Noncyclic intervals consist of meter-thick amalgamated beds of stromatolite boundstones and/or fenestral peloid wackestones and packstones that lack internal cyclicity or bedding variation but contain several sharp bedding contacts.

Controls on cycle thickness The thickness of a cycle, inclusive of its capping tidal-flat facies, can be related to several factors: (1) accommodation space (i.e., space available for sediment to accumulate, which relates the position of sea level relative to the flooded preexisting sediment surface or sea bottom), (2) rate of sediment accumulation, (3) rate of base-level change, (4) slope of the flooding surface, (5) mechanical sediment and diagenetic compaction, and (6) isostatic, thermal-tectonic, and active-fault subsidence [see also Kendall and Lerche (1988)]. In the following discussion I assume that the amplitude and the periodicity of sea-level fluctuations are similar within the study area, such that (1) sea level can be treated as a constant and eliminated as an unknown variable, (2) sedimentation rates for shallow-water carbonates are rapid enough to build up to or near sea level during successive floodings, which is valid for inner- and outer-platform strata, and (3) sufficient sediment is available to source tidal-flat and island-shoal aggradation and progradation.

The thicknesses of age-correlative Carixian–Domerian cycles are compared from selected intervals of five measured sections, which are representative of all carbonate strata across the platform and along strike of the platform (fig. 13). The data are discussed in the following sections.

Outer-platform island-shoal cycles Cycles from outer-platform island-shoal strata average 2.44 m (8.01 ft) thick for Jebel Bou Dahar (section 15, fig. 13) and 1.6 m (5.2 ft) thick for the southern Saharan platform (section 7, fig. 13). The Jebel Bou Dahar strata principally consist of grain-rich skeletal-oolite, ooid grainstone, and ooid-pisoid tepee-bedded cycles, whereas the southern platform strata are composed of ooid grainstone, skeletal-bivalve-oncolite, and ooid-pisoid tepee cycles.

The difference in the thickness of age-equivalent cycles from the outer-platform island-shoal facies belt between the two platforms indicates a difference in either the rate of compaction related to a slightly different textural composition of lithofacies or the rates of net accumulation and platform subsidence. Decompacting the average cycle thickness of the southern platform by 40%, which is high for grain-rich sediments [see Enos and Sawatsky (1981)], only increases the cycle thickness to 2.2 m (7.2 ft); this is still below the thickness (uncompacted) of the outer-platform cycles of Jebel Bou Dahar, which would decompact by less than 20% to 2.8 m (9.2 ft). Moreover, most peritidal cycles and top-truncated depositional sequences in the Central and Eastern High Atlas are capped by meteoric exposure crusts and autoclastic breccias, suggesting that each peritidal sequence ended with subaerial exposure, which inhibits appreciable sediment compaction (Shinn, 1983).

Outer-platform island-shoal cycles and inner-platform cycles The average thickness of uncompacted cycles in the platform interior of Jebel Bou Dahar (section 12, fig. 13) displays a threefold difference in thickness from the interior to the south-facing margin across a 5-km (3-mi) strike section (section 15, fig. 13). Cycles in the interior average 0.51 m (1.7 ft) (uncompacted) to 0.71 m (2.4 ft) (decompacted) using 40% decompaction as an approximation for restoring mud-rich carbonate sediments. As discussed, the cycles at the platform margin average 2.44 m (8.01 ft) thick (uncompacted). Cycles along the northern margin of the Jebel Bou Dahar platform are at least twice the thickness of inner-platform cycles deposited along the south side of the island. Cycles also vary in thickness across the southern platform, with cycles 22–40% thicker for the outer-platform facies than for the inner-platform facies, that is, the difference in average

Figure 12. Thickening-upward peloid-laminite cycles are gradational upward from underlying very thin bedded dololaminites. The dololaminite-marl cycles (a) represent upper intertidal-supratidal cycle facies, whereas complete cycles occur in the upper part of the section, with subtidal dolowackestones (b) and laminated, fenestral, dolowackestone-dolopackstone caps (c). This section is in a retrogradational bundle of inner-platform strata in the base of the southern platform (section 5, fig. 3).

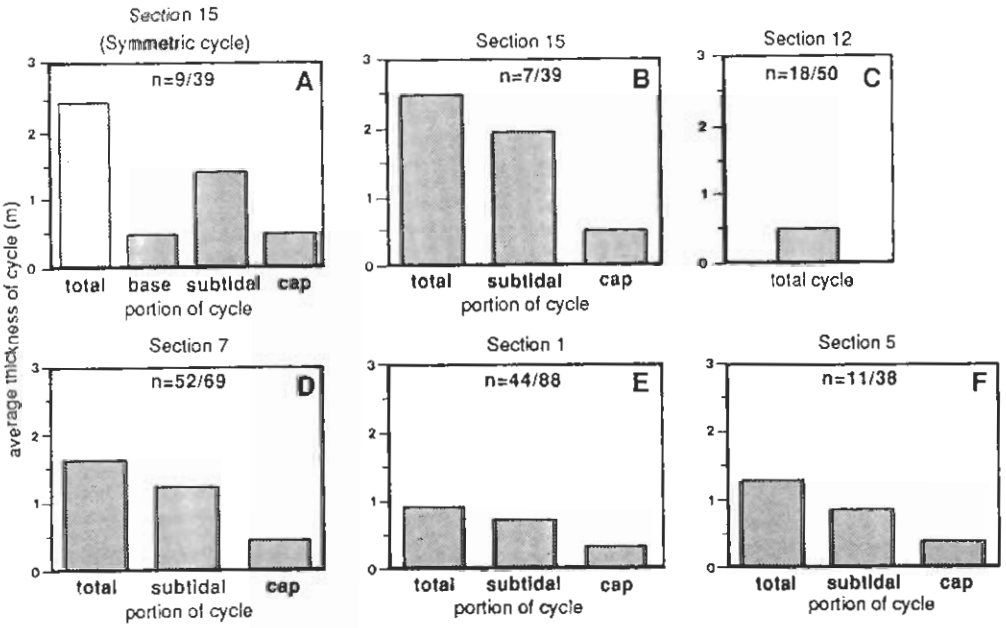

Figure 13. Comparison of the thickness of symmetric (A) and asymmetric carbonate cycles (B–F). (Top row) Outer-platform island shoal (A and B) and inner platform (C) of Jebel Bou Dahar. (Bottom row) Outer-platform island shoal (D) and inner platform (E and F) of the southern platform. *n* is number of cycles per total number of depositional units (i.e., cyclic and noncyclic strata).

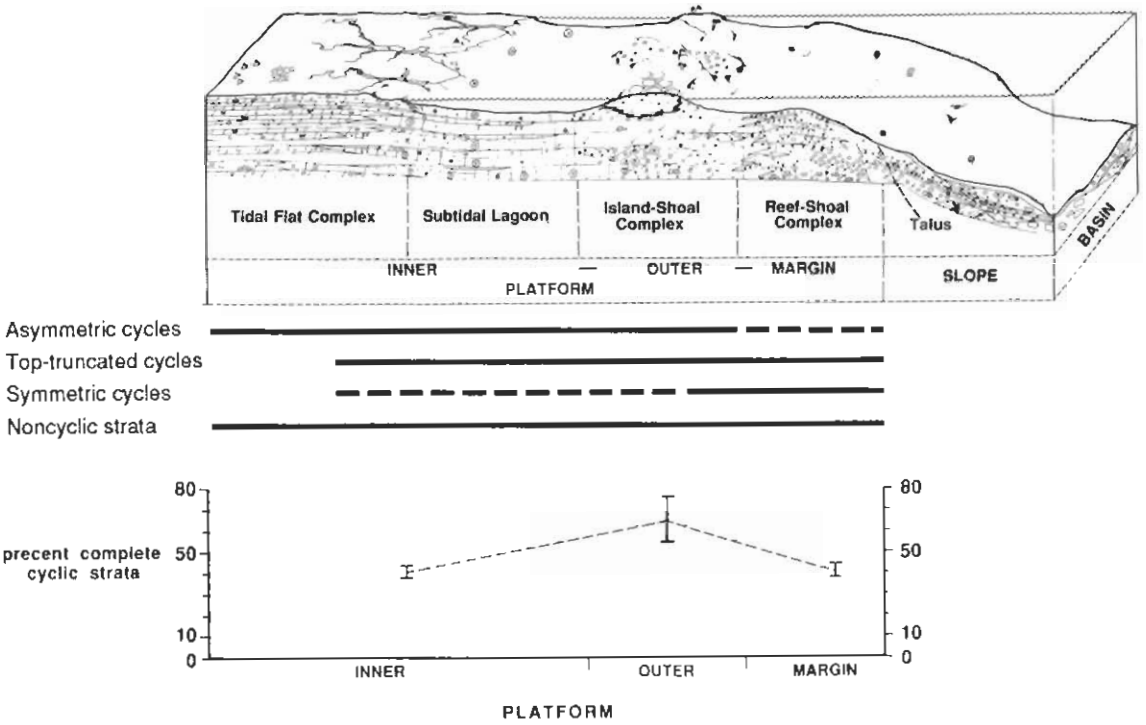

Figure 14. Distribution and percentage of peritidal cyclic and noncyclic depositional units across the platform.

thickness of sections 5 and 1 to section 7 (fig. 13) (1.25/1.6 for section 5/section 7; 0.97/1.6 for section 1/section 7).

Producing consistently thicker cycles at the margin requires more accommodation space, through either increased subsidence or sea-level rise or both, and a higher rate of net sediment accumulation. The variation in thickness is probably not gradual but more likely takes place in a steplike fashion across one and perhaps several Jurassic fault blocks that underwent syndepositional movement between the two measured sections (Crevello, 1990b).

Cyclic versus noncyclic platform strata Shallowing-upward cycles are important depositional units of the platform, but their contribution to the overall stratigraphic record of the platform can vary considerably (fig. 14). Forty percent of the outer-platform island-shoal strata along the southern margin of Jebel Bou Dahar (section 15, fig. 13) are composed of carbonate cycles (i.e., 16 of the 39 depositional units). The remaining 60% of the stratigraphic record consists of noncyclic subtidal reefs, channelized skeletal-oolite strata, and skeletal sand shoals. In contrast, nearly 76% of the outer-platform island-shoal strata of the southern platform is composed of carbonate cycles (i.e., 52 of the 69 depositional units). Symmetric cycles make up more than 50% (9 of 16) of the cycle types present in the margin of Jebel Bou Dahar, whereas no symmetric cycles were defined along the southern Saharan platform in equivalent strata. Shallowing-upward cycles make up less than 10% of platform-margin strata.

Cycles make up a greater percentage of the stratigraphic record in outer-platform strata than in inner-platform strata. This is particularly true for the southern platform, where cycles comprise between 55% (section 1) and 76% (section 7) of the stratigraphic section (fig. 13). Less than 40% (sections 5 and 12, fig. 13) of inner-platform depositional units are shallowing-upward cycles.

The decrease in abundance of cycles in a landward or inner-platform direction is related to lower net subsidence, which affects creation of accommodation space. Deposition of subtidal facies is a function of base-level rise, which with minimal subsidence and minimal sea-level rise results in few subtidal-based cycles. Instead, thin intervals of amalgamated intertidal and supratidal lithofacies of poorly developed cycles and noncyclic lithologies dominate inner-platform strata of the southern platform (section 5, fig. 13) and Jebel Bou Dahar (section 12, fig. 13).

Cycle-stacking patterns and stratigraphic bundles

Platform cycles of the Central and Eastern High Atlas typically stack with an ordered progressive shift in lithofacies, reflecting progradational, retrogradational, or aggradational

stacking patterns. The hierarchic bundling of cycles into stratigraphic packages has been described from Triassic platform carbonates (Goldhammer et al., 1987) and has been incorporated into sequence stratigraphic models (Van Wagoner et al., 1988; Read et al., this volume). Bundles of this stratigraphic order have been called megacycles (Goldhammer et al., 1987) or parasequence sets (Van Wagoner et al., 1988) and have a duration of 10^5–10^6 years [see Goldhammer et al. (this volume)].

Carbonate bundles are recognized from distant outcrop views by a characteristic weathering pattern of alternating resistant and recessive bedding (fig. 15). The intervals of resistant weathering typically are dominated by subtidal and intertidal carbonate-rich cycles. Intervals with recessive bedding correspond to stacked cycles of argillaceous limestones and shales of inner-platform, shallow subtidal, intertidal, and supratidal lithofacies.

Bundles are typically separated or bounded by recessive weathering beds, 0.5–1 m thick (1.6–3.3 ft thick), of red alluvial shale. Exposure surfaces with karst breccias are typically associated with these bounding surfaces. Although these bounding surfaces have not been correlated, their presence in platform-margin strata suggests that they are platformwide unconformities. These unconformities probably correspond to type 2 unconformities (Posamentier and Vail, 1988) or to type 1 unconformities if the entire platform was exposed. Smaller-order unconformities, here designated type 3, or marine flooding surfaces separate shallowing-upward cycles.

Bundles are composed of shallowing-upward cycles and noncyclic depositional units separated by type 3 exposure unconformities, thin beds of red shale and marl, or marine flooding surfaces. Lithofacies and cycles vary systematically within and between the bundles and often demonstrate a two-order hierarchy in stacking patterns; that is, progradational cycle-stacking patterns within a bundle characterize the overall progradational pattern of the platform. Lithofacies and cycles within bundles display minor facies shifts across cycle boundaries. In contrast, lithofacies and cycle shifts are dramatic across bounding surfaces that separate bundles. Within a bundle an upward progradational or regressive facies shift occurs in the uppermost cycles, with tidal-flat lithofacies capped by exposure surfaces. The seaward shift in facies belts and resultant subaerial exposure of the platform is followed by a major landward shift in facies belts during the ensuing transgression or base-level rise. The landward shift results in deposition of terrigenous silty shales to subtidal carbonate lithofacies over the subaerial discontinuity capping the underlying bundle.

Bundles are best developed in middle- and outer-platform strata. In restricted marine platform interiors, bundles, like the shallowing-upward cycles, are less apparent. Typically, inner-platform bundles are composed of stacked cyclic and noncyclic intertidal and tidal-flat strata that alternate with argillaceous carbonates or marl-rich noncyclic strata. The difficulty in distinguishing bundles in inner-platform strata reflects on a larger scale the same difficulty encountered in trying to distinguish amalgamated tidal-flat cycles—both are products of incomplete stratigraphic records resulting from limited creation of accommodation space.

Figure 15. Six stacked carbonate bundles (arrows) composed of shallowing-upward cycles of normal marine, inner-platform subtidal and tidal-flat lithologies. The bundles are defined by variations in bedding thickness and weathering characteristics. Resistant and thick-bedded sequences contain complete asymmetric cycles, whereas thin-bedded recessive intervals are dominated by incomplete cycles with intertidal and supratidal lithofacies. Palm trees along valley floor are approximately 5 m (16 ft) tall.

Stacking patterns of platform-margin progradational bundles Platform-margin strata of Jebel Bou Dahar and the southern Saharan platform consist of bundles 8–50 m (26–164 ft) thick (fig. 16). Vertical lithofacies successions of the progradational bundles are characterized by skeletal-dominated (coral-bivalve-algal) depositional units (cyclic and noncyclic) in the lower portion of the bundle that grade upward into ooid-dominated depositional units. The tops and bases of the bundles are defined by thin shale beds or exposure unconformities. Strata within the platform-margin bundles consist of skeletal and oolitic shallowing-upward asymmetric cycles, symmetric cycles, and top-truncated cycles. Subaerial unconformity surfaces (i.e., type 2 unconformities) are not common in platform-margin bundles because of the distally steepened margin profile. Therefore exposure of the entire platform did not occur frequently.

Stacking patterns of outer-platform progradational and aggradational bundles Outer-platform strata generally consist of well-defined stacking patterns that are separated by type 2 exposure surfaces (figs. 15, 17, and 18). Exposure surfaces are defined by thin recessive red shale beds or exposure crusts, which are characterized by autoclastic breccias and irregular microkarst surfaces. Within the progradational bundles there is a notable upward change from greater skeletal diversity in the basal cycles to more restricted marine conditions in the uppermost cycles. A reciprocal change also occurs in thickness of lithofacies, with an upward change from thick, open marine subtidal lithofacies

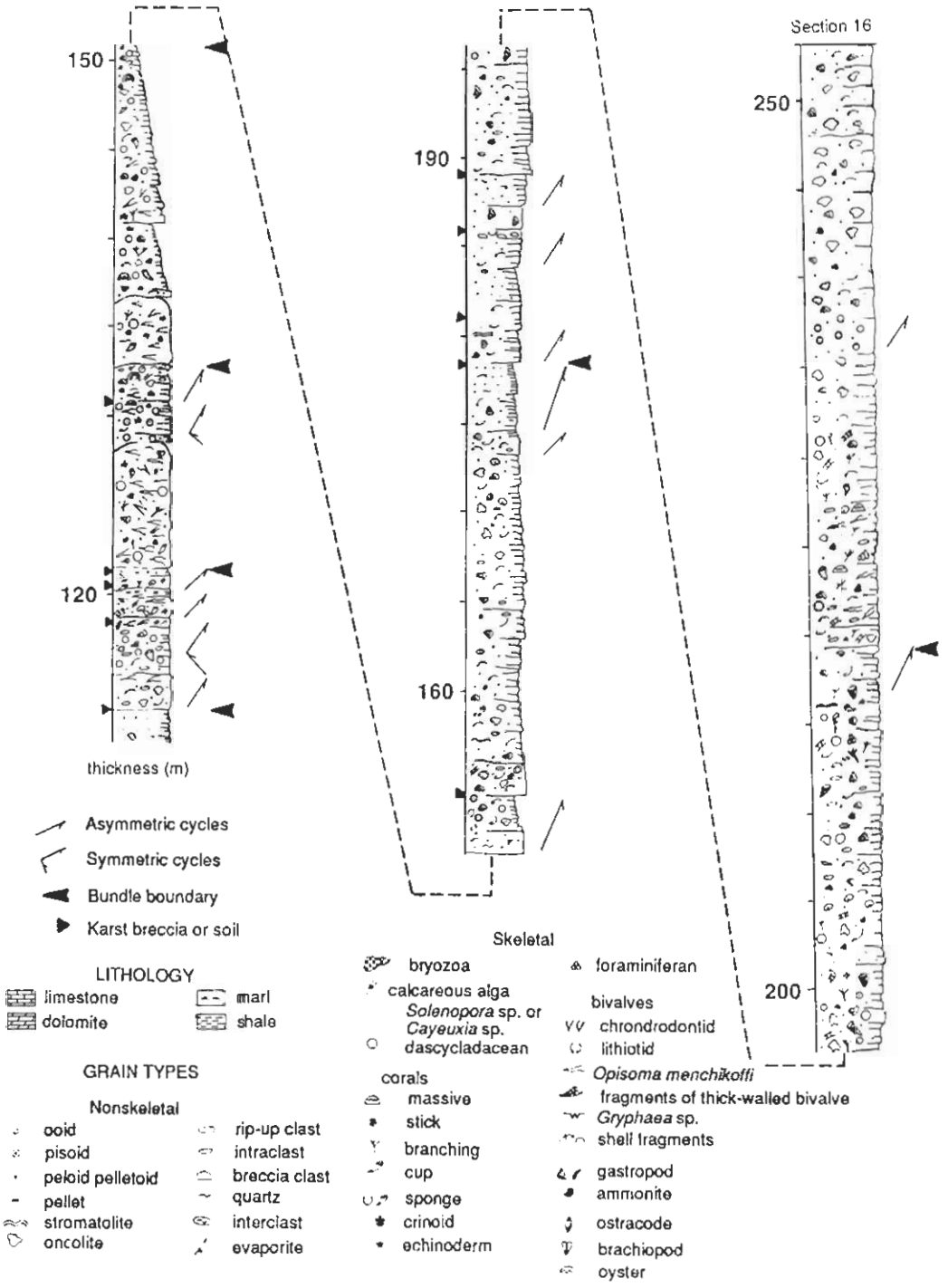

Figure 16. Stratigraphic interval from the platform margin of Jebel Bou Dahar (fig. 3, section 16, 110–255 m) (Crevello, 1990b). Section illustrates lithofacies, shallowing-upward cycles, symmetric cycles, top-truncated cycles, bounding surfaces of bundles, and karst breccias.

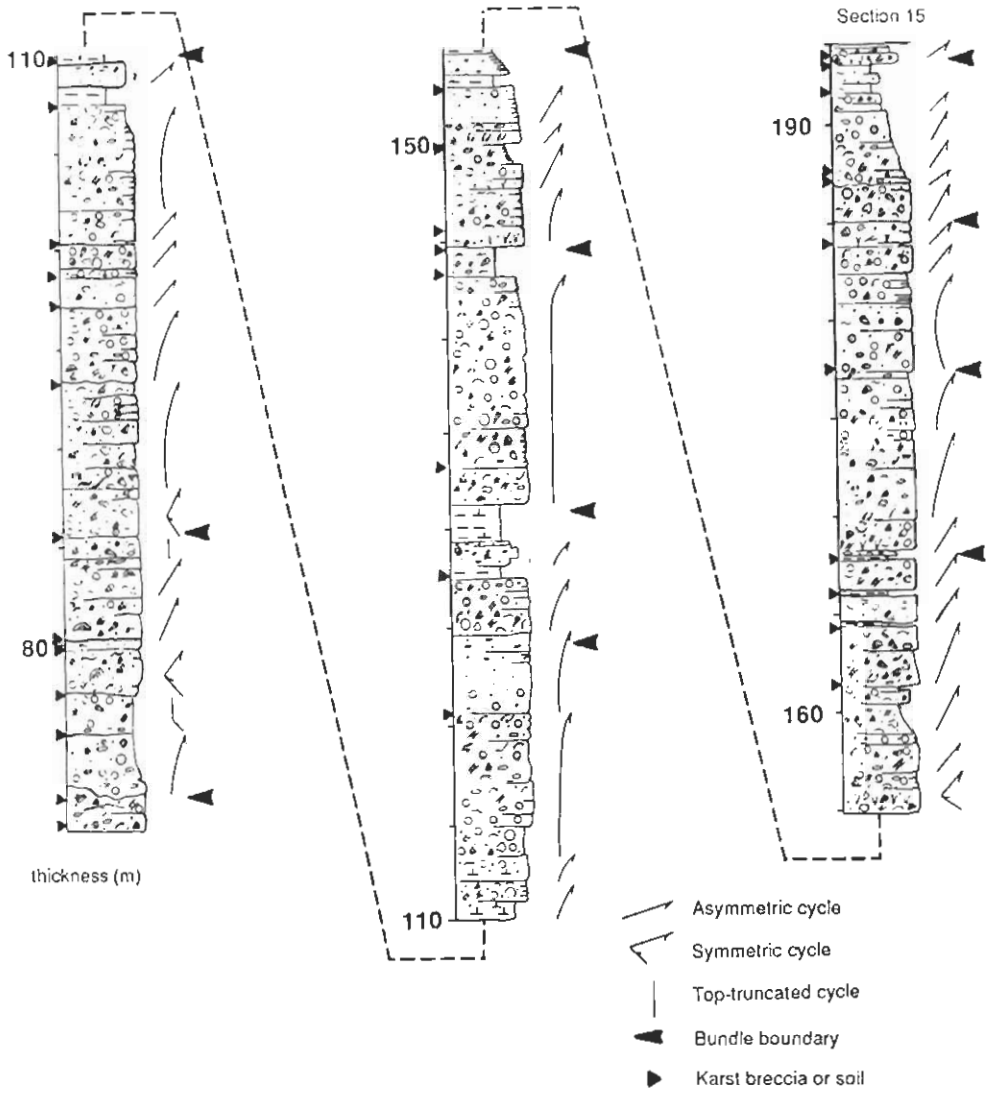

Figure 17. Stratigraphic interval from the outer platform of Jebel Bou Dahar (fig. 3, section 15, 70–195 m) (Crevello, 1990b). See fig. 16 for symbols.

and thin tidal-flat lithofacies to thin subtidal lithofacies and thick tidal-flat strata approaching the upper bounding surface of the bundle (figs. 15, 17, and 18).

In aggradational bundles shallowing-upward cycles are dominated by skeletal subtidal lithofacies and are capped by ooid shoal and channel sequences. Aggradational bundles maintain relatively constant thickness throughout the section, and upward-thinning of cycles is less apparent.

The outer-platform strata exposed at Jebel Bou Dahar contain 11 bundles in 190 m (620 ft) of Domerian and upper Carixian platform carbonates (fig. 17). Seven bundles are present in the upper 80 m (260 ft) of section 15 between 110 and 190 m (360–620 ft) (fig. 17). Below 110 m (360 ft) several major bounding surfaces that separate bundles are defined. Similarly, in the upper part of the southern platform 8 bundles are present in the upper 90 m (300 ft) of section 7 [280–370 m (920–1,210 ft)] (fig. 18). Bundles are also present through the underlying part of the southern platform.

Retrogradational to symmetric cycle-stacking patterns are locally developed in outer-platform bundles. For example, a symmetric bundle begins at the base with an argillaceous peloid wackestone cycle that grades upward into skeletal-rich lithofacies, suggesting a gradual rise in base level from the subaerial exposure represented by the underlying red shale to open marine subtidal conditions [fig. 17, section 15; 110–128 m (360–420 ft)]. The middle of the bundle is a channel sequence (i.e., a tidal channel–beach sequence) with bioclastic and oolitic lithofacies, which gradually thin upward into a capping exposure horizon. The next bundle is retrogradational, with a top-truncated cycle that

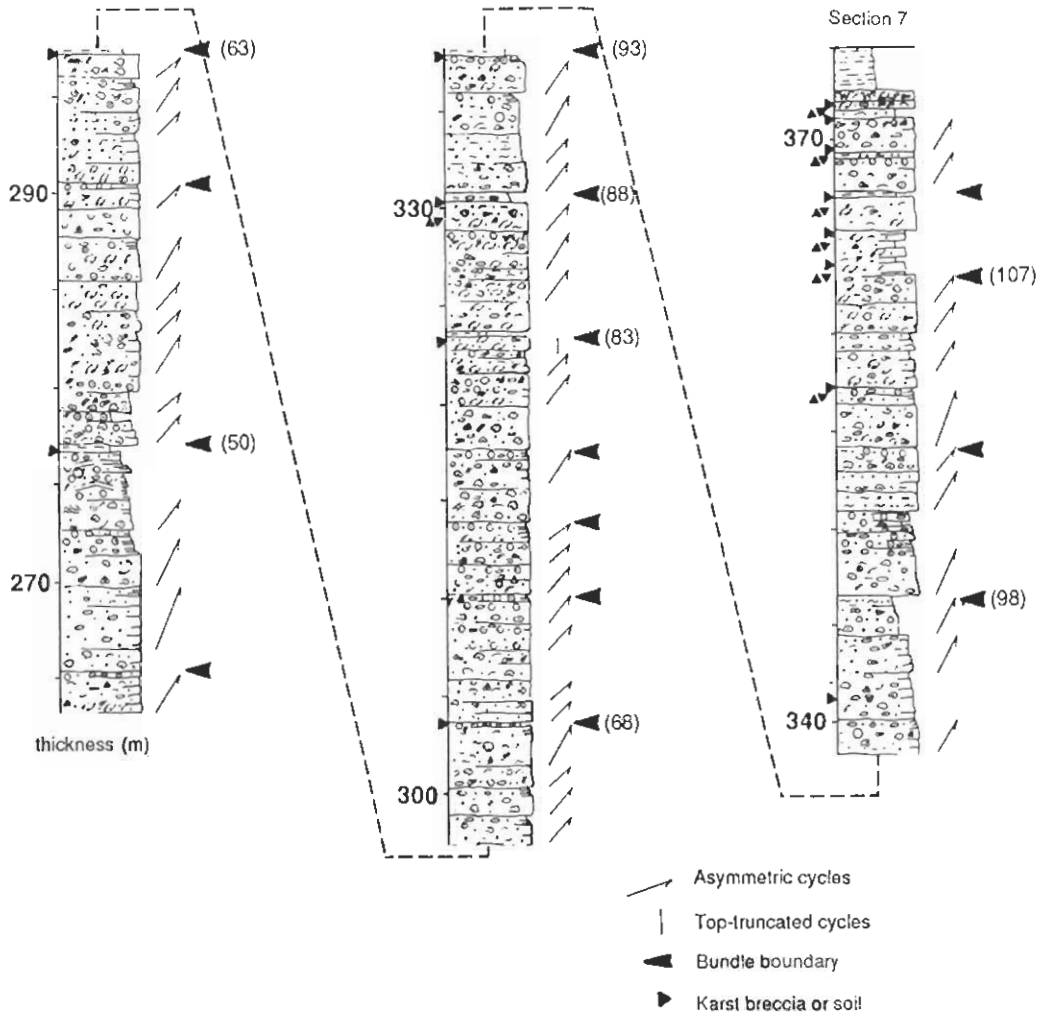

Figure 18. Stratigraphic interval from outer platform strata of the southern Saharan platform (fig. 3, section 7, 265–375 m) (Crevello, 1990b). See the Fischer plot (fig. 22) of this measured section and fig. 16 for symbols. Numbers to the right of the bounding surface arrows refer to bed numbers in figs. 22 and 26.

also contains a silty, argillaceous base but passes rapidly into a top-truncated bioclastic bed. The top-truncated bioclastic interval is overlain by a thick, crossbedded, channel-fill sequence that is capped by a type 3 exposure surface [fig. 17, section 15; base at 131 m (430 ft)]. The cycle-stacking pattern of the next overlying bundle is progradational, dominated by lithiotid bivalve banks and punctuated by several type 3 subaerial exposure surfaces [fig. 17, section 15; base 145 m (476 ft) to top 153 m (502 ft)].

Cycle-stacking patterns in the upper part of the southern platform (fig. 18) are equally variable in lithofacies and thicknesses. Bundles vary in thickness from 6 m to 15 m (20–49 ft) [fig. 18; 277 m (909 ft)] to 6–7 m (20–23 ft) thick [fig. 18; 324–331 m (1,063–1,086 ft), 331–338 m (1,086–1,109 ft)] and are bounded by type 2 exposure surfaces and recessive shale. Ooid and bivalve lithofacies are common in most bundles, although locally, silty, nonskeletal lithofacies are important [fig. 18, section 7, 331–338 m, 338–347 m, and 347–357 m (1,086–1,109 ft, 1,109–1,138 ft, and 1,138–1,171 ft)].

Stacking patterns of inner-platform retrogradational bundles Retrogradational bundles are present in the base of the Sinemurian platform of Jebel Bou Dahar and are also evident in inner-platform strata of the southern Saharan platform (figs. 19–21). The base and middle interval of the southern platform consist of thickening-upward retrogradational bundles that are composed of stacked shallowing- and thickening-upward peloid-laminite peritidal dolomite cycles. Cycles are difficult to recognize in the basal portions of the bundles, and stacking patterns typically consist of nodular marls with thickening-upward, restricted

Figure 19. Inner-platform retrogradational stacking pattern in the base of the southern Saharan platform. Retrogradational dolomite-marl and peloid-laminate cycles dominate the bundles of the lower part of the platform (a–b), and retrogradational (b–c) to progradational (above c) skeletal-bivalve-oncolite and peloid-laminite cycles dominate the middle and upper parts of the platform, respectively. Sequence boundaries (arrows) cap packages of retrogradational bundles.

Figure 20. Retrogradational stacking pattern of bundles within a depositional sequence consists of five apparent thickening- and deepening-upward carbonate bundles (1–5). Bundles are composed of shallowing-upward cycles; upper bundles (3–5) each contain two to three cycles, which are dominated by intertidal and subtidal (resistant weathering) lithofacies; bundles in lower portion of depositional sequence (1 and 2) are dominated by intertidal and tidal-flat lithofacies of nodular marls and dolomudstones (recessive weathering), which are noncyclic. Thickness of retrogradational depositional sequence is approximately 20 m (65 ft). Person for scale is standing at the base of bundle 5.

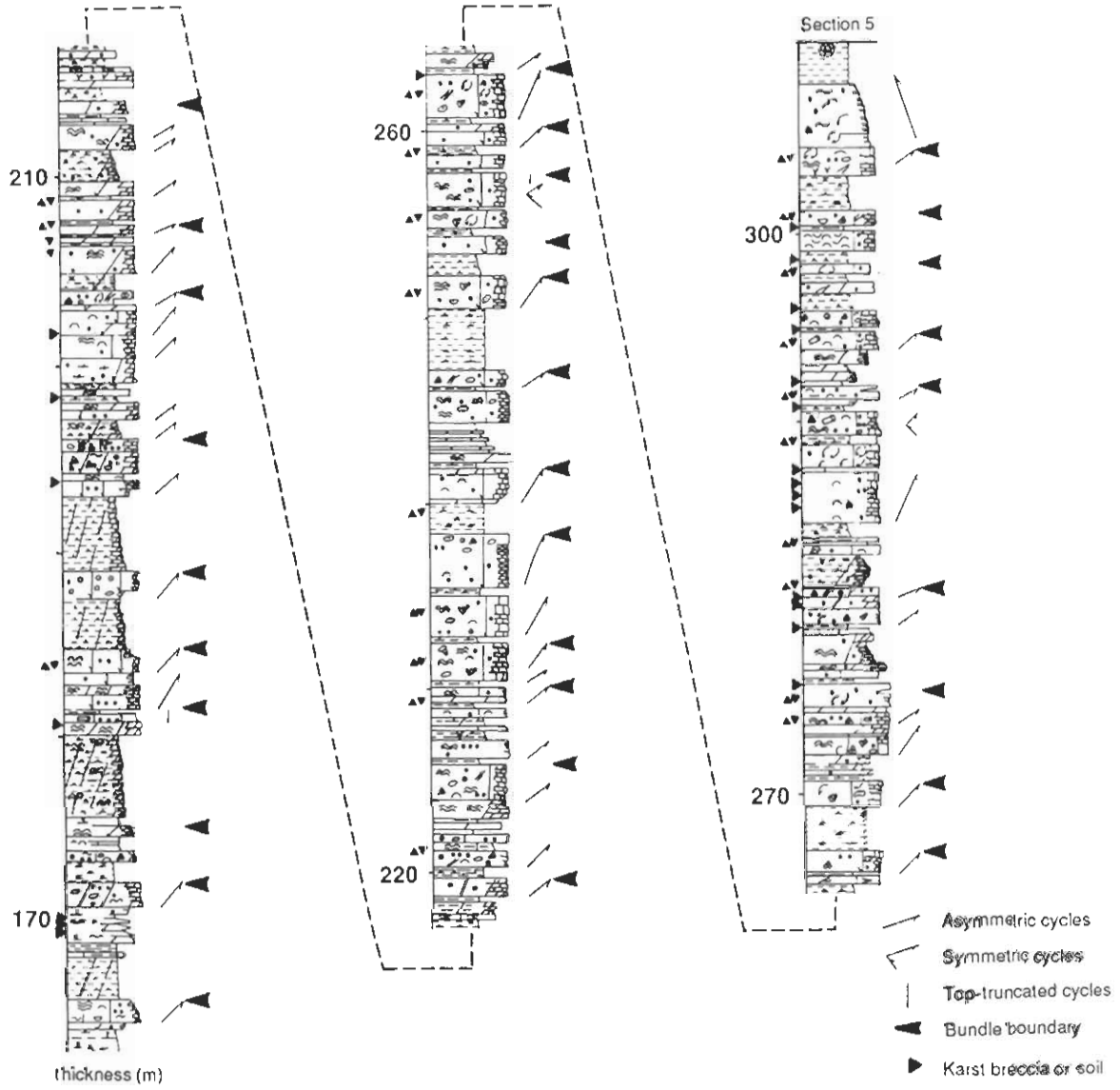

Figure 21. Stratigraphic interval from inner-platform strata of the southern Saharan platform (fig. 3, section 5, 165–310 m) (Crevello, 1990b). See fig. 16 for symbols.

marine, peloid-laminite dolomite cycles. The upper portions of the bundles consist of 4–6-m-thick (13–20-ft-thick) intervals of stacked, restricted marine, mixed limestone-dolomite, skeletal-bivalve-oncolite, and peloid-laminite cycles. The bundles display a reciprocal stratigraphic relationship, with tidal-flat lithofacies of nodular, recessive-weathering dolomites dominating the lower bundles and mixed limestone-dolomite strata dominating resistant-weathering subtidal to tidal-flat lithofacies of the upper bundles (fig. 20). In these inner-platform bundles, thick beds of resistant-weathering, crossbedded or burrowed, skeletal dolomites or limestones represent the deepest marine portion of the bundle. Top-truncated subtidal cycles occur in the upper parts of the bundles (fig. 20; see also fig. 11). The nodular marls and stromatolitic fenestral peloid dolostones in the basal portion of the retrogradational bundle represent the shallowest facies of the bundles. These bundles stack to 5–20 m (16–66 ft) thick.

Discussion

Mechanisms driving cycle-stacking patterns Depositional cyclicity is manifested in carbonate platform sequences throughout the geologic record, from Precambrian rocks to Recent sediments (Grotzinger, 1986; Hardie and

Shinn, 1986; James, 1984). In the platform strata of the High Atlas the repetitive nature of cyclicity and stacking patterns indicates that more than random processes operated to influence sedimentation patterns and stratigraphy. Several mechanisms involving either allogenic or autogenic processes have been proposed to control or influence the development of cycles within carbonate rocks.

The autogenic, or autocyclic, model invokes mechanisms that are intrinsic to the sedimentary basin, in which internal feedback produced by depositional processes controls cyclicity (Ginsburg, 1971). Autocyclic processes are of several types: area-diminishing sediment source (Ginsburg, 1971), internal sediment redistribution (Pratt and James, 1986), sediment compaction, and subsidence. A common autogenic process in terrigenous clastic settings is distributary delta switching.

Allocyclic mechanisms rely on extrinsic mechanisms to drive the sedimentary system and cause cyclicity (Fischer, 1964; Grotzinger, 1986); such mechanisms include episodic regional subsidence and sea-level fluctuations. Differentiating between the mechanisms is equivocal because autocyclic processes, such as those recognized by Ginsburg (1971), can produce the same sedimentary record as allocyclic episodic subsidence (Goldhammer et al., 1987). However, by using passive margin subsidence rates of 1.7–5.4 cm/1,000 years, Koerschner and Read (1989) argued that subsidence does not create sufficient accommodation space within 20 k.y. for autocyclic cycle development. As a consequence, the orbital-forcing model and its influence on glacioeustasy have been invoked as the major control on carbonate cyclicity for Precambrian to Recent strata (Grotzinger, 1986; Read et al., 1986; Goldhammer et al., 1987).

Allocyclic orbital forcing on glacioeustasy is the only viable mechanism, other than pulsating yo-yo tectonics, that can explain subaerial exposure of marine and intertidal sediments (Goldhammer et al., 1987). Exposure of subtidal sediments requires a base-level fall below the depositional surface of marine sediments. Episodic or constant subsidence would tend to favor sediment aggradation to sea level, but without any possibility for exposing the sediments to subaerial diagenesis.

Orbital forcing of the earth's climate results from perturbations in orbital precession, obliquity, and eccentricity, which directly affect solar insolation and the formation of ice sheets and sea melt and ultimately drive glacioeustatic fluctuations in sea level. In the absence of continental ice sheets, thermal insolation linked to time-variable orbitally forced solar radiation can also produce sea-level fluctuations through thermal expansion or contraction of the ocean surface layers, but this can account for only a few to 10 m (30 ft) of sea-level change.

Orbital forcing of high-frequency stratigraphy may be manifested in the number of cycles developed per bundle (megacycle or parasequence set). For instance, a ratio of approximately 5:1 cycles per megacycle was used by Goldhammer et al. (1987) to support an orbital forcing in which the 20-k.y. precession controls cycles and the 100-k.y. short eccentricity dictates the stacking patterns of megacycles. In contrast, Goldhammer et al. (this volume) have proposed a 10:1 (or 400 k.y./40 k.y.) cyclicity of long eccentricity and obliquity for Pennsylvanian cycles of the Paradox basin.

The main spectra of orbital frequencies calculated within the Milankovitch band that are proposed to affect stratigraphy include precession, $P = 20$ (18–23) k.y.; obliquity, $O = 40$ k.y.; short eccentricity, $E_1 = 100$ k.y.; and long eccentricity, $E_2 = 400$ k.y. (Hays et al., 1976; Berger, 1980; Imbrie et al., 1984; Fischer, 1988). Eccentricity by itself is not considered an important driving mechanism of sedimentary cyclicity (Fischer, 1988). Instead, as demonstrated through stratigraphic studies and modeling, combinations of precession, obliquity, short eccentricity, and long eccentricity are believed to control cycle ratios and stacking patterns (Fischer, 1988; Goldhammer et al. 1987, 1990).

Cycle duration Estimates of the duration of cycles and bundles are often applied to demonstrate a relationship with Milankovitch rhythms (Fischer, 1964; Grotzinger, 1986; Read et al., 1986; Goldhammer et al., 1987, 1990). Fischer first proposed a 50-k.y. average duration for Triassic Löfer peritidal cycles. Fischer divided the total number of cycles in the platform by the approximate age of the platform sequence to derive an average duration for each cycle. Using time-series analyses, Goldhammer et al. (1987) revised the length of Fischer's cycles to 20 k.y. for individual cycles and 100 k.y. for megacycles. Grotzinger (1986) estimated cycle lengths for Precambrian carbonates of 18–53 k.y. Although these estimates vary considerably, Grotzinger (1986) emphasized that the durations of cycles are all of the order of 10^4 years, which is within the range proposed for Milankovitch orbitally forced perturbations. The underlying assumption in applying a Milankovitch climate-forcing model to stratigraphic cyclicity is that the celestial mechanics of the sun-earth system, which govern the orbital perturbations of the earth, have been in effect since the Precambrian, even though the durations and intensity of these perturbations may have changed through geologic time.

In this study the average durations of small-scale shallowing-upward cycles were estimated from four measured sections (table 1). Using an average age for the Liassic stages, I calculated individual carbonate cycles to range in duration from 24 k.y. to 129 k.y. (table 1). Outer-platform strata vary less in cycle duration, 24–33 k.y. (table 1, section 7), compared with inner-platform strata in which individual cycles range from 40 k.y. to 129 k.y. (table 1, sections 5 and 12) or transitional outer-platform margin strata in which cycles range from 27 k.y. to 119 k.y. (table 1, section 15). The duration of cycles in outer-platform strata are believed to reflect more accurately the lengths of individual cycles because a more continuous and complete stratigraphic record is preserved along with better biostratigraphic age control.

Table 1. Duration of carbonate cycles

Section	Number of Cycles	Duration (m.y.)	Age Range (years/cycle)	Stage
15	67	6–8	89,600–119,400	Carixian–Domerian
		3–4	44,800–59,700	Late Carixian–Domerian
		2.5	37,300	Domerian
7	241	6–8	24,900–33,200	Carixian–Domerian
5	140	12–16	85,700–114,300	Sinemurian–Pliensbachian
		6–8	42,900–57,100	Pliensbachian
12	62	6–8	96,800–129,000	Pliensbachian

Thus the range of 24–33 k.y. is believed to be the best approximation for the duration of the Liassic carbonate cycles. This estimate is well within the range of the 20–40-k.y. duration assigned to the frequencies of orbital precession and obliquity.

Cycle and bundle periodicities Cyclic stratification has often been used to support climatic and/or glacioeustatic signals in marine and lacustrine strata, even though cyclicity is not necessarily a corollary for periodic sedimentation (Kominz and Bond, 1990). Inaccurate time scales and limited understanding of the relationship between sedimentation and accumulation rates result in imprecise calculations of cycle durations. Methods of spectral analysis test the periodicity of cyclic strata by assigning time or thickness to the sequence and by analyzing for frequency distributions that fall within the Milankovitch band of 19–400 k.y., in which case orbital modulation is invoked to control the stratification cycles. The methods include time-series analysis (Schwarzacher, 1964), Walsh analysis (Weedon, 1986), autocorrelation (Goldhammer et al., 1987), maximum entropy series analysis (MESA) (Goldhammer et al., 1990, this volume), and the gamma method (Kominz and Bond, 1990). Stratification spectra that do not correspond to the Milankovitch bands of orbital forcing are used as support for nonperiodic, random autogenic processes (Dunn et al., 1991).

Autocorrelation of the Carixian–Domerian stacking pattern supports the field observations that stratification bundles from the outer platform, where the sedimentary record is believed to be most complete, consist of 5 cycles per bundle (fig. 22). MESA and autocorrelation spectra support a hierarchic bundling of 20:5:1, which corresponds to long (E_2) and short (E_1) eccentricity and precession (P) bundling (fig. 23). Tuning the MESA spectral clusters to a precession of 18 k.y. demonstrates power spectra at 396 k.y. (E_2) and 118 k.y. (E_1). The spectra at 79 k.y. and 61 k.y. are believed to be related to either combined signals of precession and obliquity or, more likely, an incomplete record of cycle preservation or nondeposition by missed beats (Schwarzacher, 1987; Goldhammer et al., 1990).

Walsh spectral analysis (fig. 24) was applied to the same interval of section 7 as the MESA correlation (fig. 23). The Walsh and MESA analyses give similar results, although more spectral clusters are identified using the Walsh analysis, which reflects the difference between the continuous MESA and the discontinuous Walsh spectra analyses [see Weedon (1986)]. Both methods demonstrate cycle ratios near 20:1 and 5:1, and the autocorrelation indicates cycle ratios of 5:1. Additional cycle ratios of 9:1 and 32:1 were identified from the Walsh analysis, which, if related to orbital forcing and tuned to 18 k.y., yields 173-k.y. and 576-k.y. intervals, respectively. The 10:1 (i.e., 9.6) cycle ratio may reflect obliquity and long eccentricity, but the cause for the 32:1 cycle ratio is uncertain.

Discrepancies between spectra of astronomical cycles and sedimentary sequences do not preclude orbital forcing because little is known about the mechanism that links orbital variations to climate and climate to sedimentation (Schwarzacher, 1987). Ideal conditions with a complete sedimentary record would result in cycle ratios of 20:5:1 for E_2:E_1:P or 10:1 for E_2:O ratios. If cycles have been missed either in counting or by nondeposition, then the reduced cycle number would appear to give a duration that is too long for the cycles. This implies that, if the choice is between a cycle with a duration of 40 k.y. or one with a duration of 100 k.y., the 40-k.y. duration is more likely (Schwarzacher, 1987).

Amplitudes and orders of sea-level oscillations The amplitudes of sea-level oscillations are interpreted from reconstructions of the platform-top gradient and the depth to the shelf-slope break. The platform-top gradient was calculated by the difference in cycle thicknesses between the inner- and outer-platform strata. A negligible slope of 0.32–0.39 m/km (1.7–2.1 ft/mi) is calculated for the platform top at Jebel Bou Dahar [the difference in cycle thickness between sections 12 and 15 (figs. 3 and 13), viz., 1.61–1.93 m (5.28–6.33 ft) over a distance of 5 km (3.1 mi)]. Therefore a sea-level drop of only 2–3 m (7–10 ft) would expose most of the platform facies belts landward of and including the outer-platform island-shoal complex. The fall would be less if subsidence also influenced cycle thickness. Deeper lagoon sediments might remain submerged during minor sea-level fluctuations. These low-amplitude, 2–3-m (7–10-ft) sea-level fluctuations, interpreted to be precession cycles based

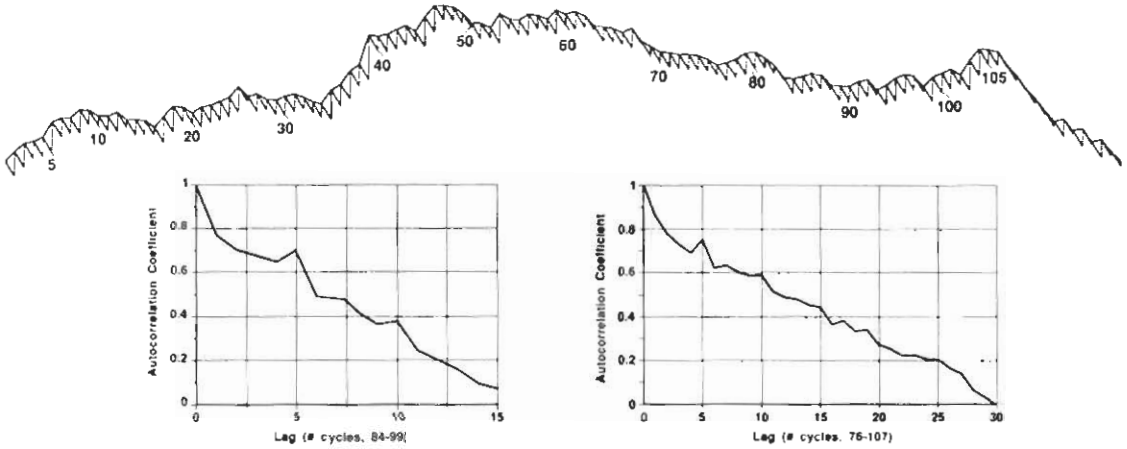

Figure 22. Fischer plot of section 7 (fig. 3) and autocorrelation (graphs) for cycles 84–99 and 76–107 (see also fig. 18). Autocorrelation indicates 5:1 cycle ratio for these overlapping intervals.

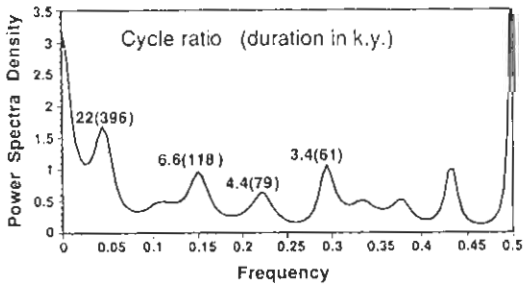

Figure 23. MESA spectra distribution of section 7 (fig. 3), cycles 1–107, of the Fischer plot in fig. 22. Cycle ratio and durations tuned to 18 k.y. are shown.

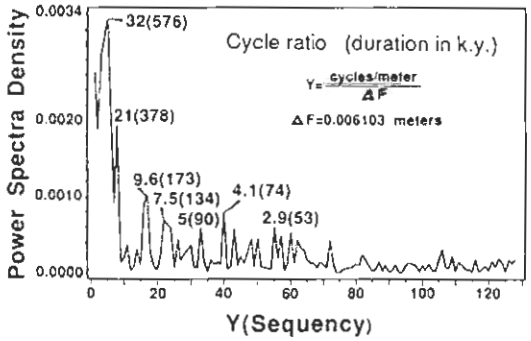

Figure 24. Walsh spectra distribution of section 7 (fig. 3), cycles 1–107, of the Fischer plot in fig. 22 (see also fig. 18). Cycle ratio and durations tuned to 18 k.y.

on spectral analysis, caused subaerial exposure of cycles within outer- and inner-platform bundles and represent type 3 and possibly type 2 unconformities.

Sea-level falls of more than 10 m (30 ft) were also important, as indicated by subaerial exposure of platform-margin reefs and ooid-skeletal shoal lithofacies. Drops of these greater amplitudes, though, were not as frequent as those recorded in the outer- and inner-platform cycles. Relatively few unconformities were identified in platform-margin strata. Therefore *low-amplitude* sea-level fluctuations affecting the inner- and outer-platform strata and formation of cycles and type 3 unconformities did not expose the entire platform. However, less frequent, cyclic, *high-amplitude* sea-level fluctuations did expose nearly the entire platform, producing the bounding surfaces of some of the bundles.

The amount of sea-level fall for high-amplitude fluctuations is difficult to document. There are only two data that can be used to gauge the amount of sea-level fall: the platform top and the depth at the margin-slope break, which occurs 40–60 m (130–200 ft) below the platform top (Crevello, 1990b; Kenter and Campbell, 1991). Therefore, with an approximate depth of 40–60 m (130–200 ft) for the distally steepened margin-slope break, a minimum fall of 10–30 m (30–100 ft) would be required to expose shallow shoals and platform-margin reefs.

Cycle-stacking patterns: An interplay of orbital forcing and subsidence

Ideal depositional sequence model The high-frequency cycle-stacking patterns and depositional sequences were controlled by the interplay of threefold hierarchy of orbital forcing, which resulted in a 20:5:1 stratigraphic bundling, and by subsidence. Modeling an ideal depositional sequence with the stacking pattern spectra of 20:5:1 requires 3 superimposed sea-level curves with amplitudes of approximately 15–30 m (50–100 ft) (E_2, 360–400 k.y.), 4–5 m (13–16 ft) (E_1, 90–100 k.y.), and 1–2 m (3–7 ft) (P, 18–20 k.y.). An ideal depositional sequence produced by the superimposed curves is composed of four carbonate bundles, or parasequence sets,

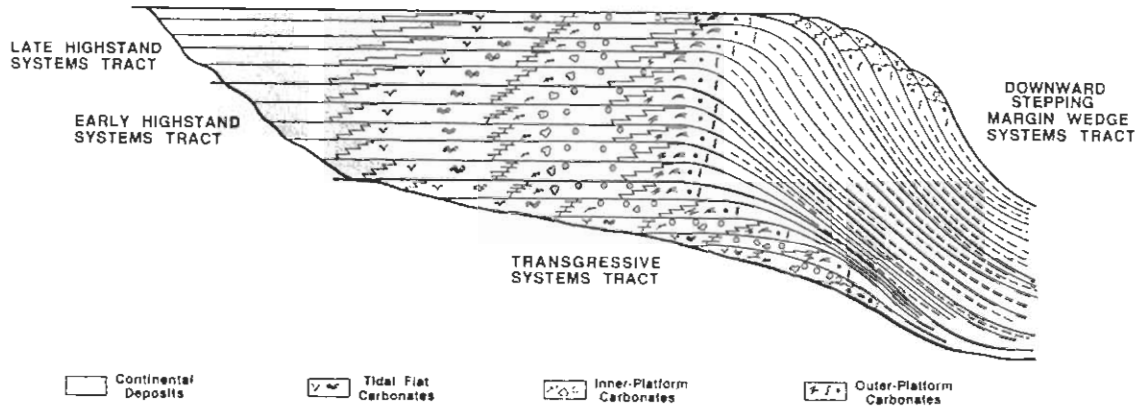

Figure 25. Depositional sequence model showing distribution of systems tracts and stacking patterns controlled by orbitally forced eustasy of three superimposed sea-level cycles of long (360 k.y.) and short (90 k.y.) eccentricity and precession (18 k.y.). High-frequency stacking pattern results in a cycle ratio of 20:5:1.

which correspond to the transgressive, early and late highstand, and margin wedge systems tracts (fig. 25) [see Read et al. (this volume)]. The ideal model consists of retrogradational cycle-stacking patterns in the transgressive systems tract, aggradational to progradational cycle-stacking patterns in the highstand systems tract, and progradational to downward-stepping lowstand shelf-margin wedge systems tract. The boundaries between the systems tracts and lithofacies offsets between the cycles are gradational because of low-amplitude sea-level fluctuations. Type 3 unconformities and correlative marine flooding surfaces separate the cycles and systems tracts in this model. These low-order, areally restricted unconformities cap most cycles and increase in number and extent in the late highstand systems tract, immediately beneath the sequence boundary, and in the basinward-stepping margin wedge systems tract.

Lithofacies offsets are most dramatic across sequence boundaries, which separate the late highstand systems tract from the shelf-margin wedge and overlying transgressive systems tracts. A sequence model driven by low-amplitude sea-level fluctuations does not develop a pronounced lowstand systems tract, which is in contrast to the high-frequency high-amplitude sea-level fluctuations that affected Pleistocene stratigraphy and which is presented in the terrigenous clastic and carbonate sequence stratigraphic models (Van Wagoner et al., 1988; Sarg, 1988).

The long-term stacking patterns and the development and distribution of systems tracts within depositional sequences are controlled by the interplay of long-term eccentricity (i.e., E_2, E_3) and subsidence. The stacking patterns and systems tracts of the ideal model (fig. 25) are controlled by long eccentricity with constant or gradually decreasing subsidence at the same periodicity as eccentricity. Depositional sequences dominated by retrogradational stacking patterns, such as the platform strata in the lower portion of the platform (see figs. 19 and 20), result from the interplay of diminishing long eccentricity and gradually increasing subsidence pulses that are equal to or greater than the period of eccentricity.

Calibrated data set Cycle-stacking patterns displayed as Fischer plots calibrated with lithofacies provide a method for demonstrating sequence boundaries and systems tracts determined from field data, approximating relative sea level or net accommodation space, and calibrating field data for stratigraphic modeling (fig. 26) (see also Read and Goldhammer, 1988; Read et al., this volume; Goldhammer et al., 1990). Major subaerial exposure boundaries and the types of cycles are located on the Fischer plot of section 7 (fig. 26), which is dominated by outer-platform strata. The strata within the platform are dominated by highstand systems tracts separated by subaerial unconformities with minor karst development. Transgressive systems tracts are rare, and margin wedges are defined by seaward facies shifts represented by nonskeletal lithofacies. In contrast, the top of the platform is capped by a sequence boundary with a well-defined stacking pattern and facies succession of a transgressive systems tract.

The top of the platform is capped by a major sequence boundary of either a type 1 or a type 2 unconformity (fig. 26, cycles 108–112). The sequence boundary is characterized by extensive karst brecciation with dramatic facies shifts across the unconformity. Beneath the sequence boundary, bundles are characterized by seaward-stepping progradational cycles of mixed skeletal-bivalve-oncolite and peloidal-laminite lithofacies. In contrast, above the unconformity the transgressive systems tract is composed of landward-stepping retrogradational, top-truncated cycles of peloid-ooid and then coral-skeletal lithofacies. The sequence boundary correlates with regional exposure during the Domerian (*Margaritatus* zone) of Atlas rift platforms and simultaneous deposition of a basin-floor wedge (Crevello, 1990a–c). Plat-

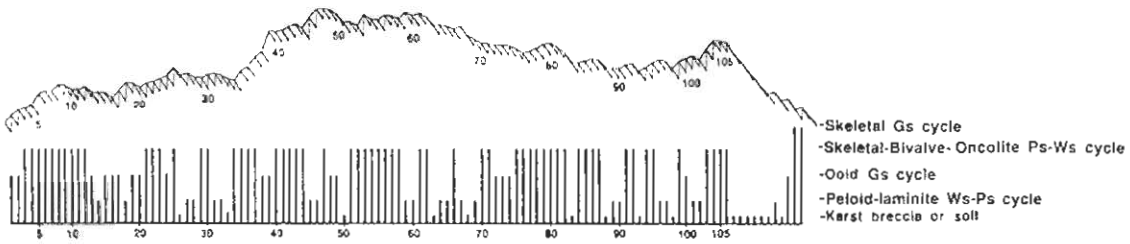

Figure 26. Bar graph distribution of cycle types plotted against the Fischer plot of fig. 22 (see also fig. 18). Systems tracts and sequence boundaries are discussed in the text. See fig. 5 for definition of abbreviations.

form exposure and deposition of the wedge are believed to have resulted from a high-amplitude fall in sea level that was probably greater than 30 m (100 ft) (Crevello, 1990b). The overlying coral-skeletal lithofacies precedes a drowning sequence of middle Toarcian age (*Bifrons* through *Falciferum* zones), which has been recognized throughout the Mediterranean (Jenkyns et al., 1985; Haq et al., 1988; Crevello, 1990a–c).

Beneath the sequence boundary, 9 type 1 or type 2 boundaries were defined within the upper 160 m (525 ft) of the platform (fig. 26, at cycles 26, 33, 50, 63, 68, 83, 88, 93, and 98). The unconformities within the platform are less dramatic than the capping sequence boundary and were defined in the field by pronounced changes in lithofacies, cycle type, and cycle-stacking patterns across subaerial exposures. The boundaries occur on the falling limbs of the cumulative thickness plots displayed on Fischer graphs [see Read et al. (this volume) and Read and Goldhammer (1988)]. In section 7, for instance, at cycle 33 (fig. 26) nonskeletal, peloidal lithofacies dominate the cycles below the unconformity, whereas mixed skeletal-peloidal cycles characterize the cycles above the boundary. Cycles thicken above the boundary at cycle 33, which is characteristic of transgressive systems tracts. Boundaries at cycles 68 and 88 are defined more by lithofacies variations across the exposure boundary than by cycle-stacking patterns.

Carbonate bundles dominated by cycles with mixed skeletal-oolitic and skeletal-peloidal lithofacies are interpreted as highstand systems tracts, especially when the sequence overlies nonskeletal lithofacies. Their distribution within the sequence is variable. In the sequence between cycles 5 and 26 (fig. 26), the basal cycles or early highstand systems tract is composed of skeletal and oolitic lithofacies, whereas the late highstand systems tract is dominated by oolite and peloid cycles. Similarly, the highstand systems tract at cycles 39–44 is composed of skeletal and peloidal cycles that pass into late highstand systems tract oolitic cycles at cycles 45–50. In contrast, the overlying highstand systems tract is dominated by skeletal cycles with few oolite cycles. Nonskeletal lithofacies dominate two bundles; one is above cycle 88, which has a retrogradational facies succession, and the other is a progradational bundle above cycle 93. These two nonskeletal-dominated bundles correspond to a low on the Fischer plot curve and represent late highstand and margin wedge systems tracts, even though the cycle thicknesses are rather constant above and below the type 2 boundary.

The observed cycle ratios for the field-calibrated Fischer plots of the high-frequency depositional sequences range between the 7:1 and 16:1 cycles, which contrasts with the statistical analyses of long-term cycle-stacking ratios of 20:1. The discrepancy between the field data and the statistical data reflects two fundamental stratigraphic problems: (1) the visual observation of picking all unconformities as sequence boundaries, which is an incorrect assumption because type 2 and type 3 unconformities may separate the early from the late highstand systems tract or the margin wedge systems tract from the transgressive systems tract, whereas the sequence boundary is defined between the late highstand systems tract and the margin wedge systems tract; and (2) the aspect of stratigraphic hiatus or missing cycles through nondeposition during seaward shifts in systems tracts. The Fischer plot in this example defines the systems tracts but only when cycle lithofacies are used to demonstrate facies and systems tract shifts; it does not discriminate between type 2 and type 3 unconformities, nor does it record missing strata. The divergence from an ideal sequence model also suggests that the variable controlling the long-term bundling is more complex than a threefold orbital-forcing mechanism, and it is likely that variable and aperiodic subsidence is an important control on long-term platform stacking patterns and stratigraphy within the High Atlas basin.

Conclusions

Orbital forcing and subsidence were the dominant controls on high-frequency cycles and stacking patterns observed in Jurassic platform strata from the Central and Eastern High Atlas rift. Field observations supported by time-thickness and spectral analyses of stacking patterns and cycle ratios in outer-platform strata demonstrate a threefold superimposed cyclicity of 20:5:1. The cycle ratio supports orbital forcing on high-frequency stacking patterns with periodicities of long eccentricity, short eccentricity, and precession cycles, which

approximate rhythms of 360–400 k.y., 90–100 k.y., and 18–21 k.y., respectively. The amplitudes of the superimposed sea-level curves were estimated as 15–30 m (50–100 ft) for the long eccentricity, 4–5 m (13–16 ft) for short eccentricity, and 1–2 m (3–7 ft) for precession. The amplitude estimates are based on the nature and distribution of cycles, stacking patterns, and exposure surfaces. Divergence of Jurassic stacking patterns from an ideal depositional sequence, driven by three superimposed sea-level cycles, indicates that both variable long eccentricity and subsidence combined to control the character of progradational, aggradational, and retrogradational cycle-stacking patterns and the stacking patterns of systems tracts at the scale of depositional sequences.

High-frequency sea-level fluctuations were the dominant control on the development of individual carbonate cycles, although subsidence had a secondary effect on thickness. The variability in the record of cyclicity across the platform, with outer-platform strata containing the highest percentage of cyclicity (75%) and the platform margin or interior having less than 50% cyclic strata, is related to the interplay between subsidence and high-frequency but, more important, *low-amplitude* sea-level fluctuations. In contrast, local intrinsic factors, such as platform-top gradient and depth to storm wave base, influenced the internal lithofacies characteristics of cycle symmetry.

The question remains for every case study of whether the cycles, stacking patterns, and systems tracts distribution within depositional sequences are determined by local sediment supply and subsidence or by global processes that affect ocean basin or seawater volumes. In this study the combination of high-quality stratigraphic data sets, which were scrutinized by time-depth and time-series analyses of stacking patterns and cycle ratios, enabled investigations of the controls on carbonate platform strata. In the absence of superb outcrop exposures, such as those of the Jurassic High Atlas, the ability to quantitatively analyze real stratigraphic data would be diminished, as would be the ability to investigate the controls on stratigraphic sequences and to constrain stratigraphic modeling.

Acknowledgments I would like to thank the Marathon Oil Company for allowing me to conduct and publish this study. The cooperation of the Moroccan Geological Service, in particular, Mohammed Bensaid and Mohamed Dahmani, is acknowledged. The content of this paper was improved through discussions and manuscript reviews by colleagues P. Choquette, E. Franseen, R. Inden, C. Kendall, and J. Warme. R. Farrar, R. Goldhammer, and D. Watts are acknowledged for their discussions and illustrations of Fischer plots and spectra analyses. G. Wilkinson and B. Sikora drafted the illustrations.

References

Agard, J., and Dresnay, R., 1965, La region mineralisée du Jebel Bou Dahar pres de Beni Tajjite (Haut Atlas oriental)—étude géologique et metallogenique; *in*, Colloque sur des Gisements Stratiformes de Plomb, Zinc, et Manganese du Maroc, Agard, J., and Diouri, M., eds.: Service Géologique du Maroc, Notes and Memoires 181, p. 132–152

Berger, A., 1980, The Milankovitch astronomical theory of paleoclimates—a modern review: Vistas in Astronomy, v. 24, p. 103–122

Bond, G. C., Kominz, M. A., Steckler, M. S., and Grotzinger, J. P., 1989, Role of thermal subsidence, flexure, and eustasy in evolution of early Paleozoic passive margin carbonate platforms; *in*, Controls on Carbonate Platform and Basin Development, Crevello, P. D., Wilson, J. L., Sarg, J. F., and Read, J. F., eds.: Society of Economic Paleontologists and Mineralogists, Special Publication 44, p. 39–62

Burri, P., du Dresnay, R., and Wagner, C. W., 1973, Tepee structures and associated diagenetic features in intertidal carbonate sands (Lower Jurassic, Morocco): Sedimentary Geology, v. 9, p. 221–228

Crevello, P. D., 1988, Carbonate platform facies of the southern margin of the Central High Atlas rift; *in*, Evolution of the Jurassic High Atlas Rift, Morocco—Transtension, Structural and Eustatic Controls of Carbonate Facies, Tectonic Inversion, Warme, J. E., ed.: American Association of Petroleum Geologists, Mediterranean Basins Conference, FieldTrip 9, p. X-1–X-42

_____, 1990a, Depositional systems tracts, stacking patterns, and sequence stratigraphy of Lower and Middle Jurassic synrift carbonate platforms, Central and Eastern High Atlas, Morocco (abs.): International Association of Sedimentologists, 1990 Annual Meeting, Proceedings with Abstracts, p. 111–112

_____, 1990b, Stratigraphic evolution of Lower Jurassic carbonate platforms—record of rift tectonics and eustasy, Central and Eastern High Atlas, Morocco: Ph.D. dissertation, Colorado School of Mines, Golden, 456 p.

_____, 1990c, Termination of carbonate platforms—eustatic fluctuations in base level (abs.): American Association of Petroleum Geologists Bulletin, v. 74, p. 635–636

Crevello, P. D., Warme, J. E., Septfontaine, M., and Burke, R. B., 1987, Evolution of Jurassic carbonate platforms in an active transtensional rift—High Atlas of Morocco (abs.): American Association of Petroleum Geologists Bulletin, v. 71, p. 543–544

du Dresnay, R., 1979, Sediments jurassiques du domaine des chaines atlasique du Maroc; *in*, Symposium Sedimentation Jurassique West Europeen: Association Sedimentologistes Français, Special Publication 1, p. 345–365

Dunn, P. A., Goldhammer, R. K., Hardie, L. A., and Nguyen, C. T., 1991, Two-dimensional forward modeling of Lower Ordovician platform carbonate sequences (Beekmantown Group, central Appalachians)—the search for high-frequency autocycles (abs.): American Association of Petroleum Geologists, Annual Meeting, p. 101

Fischer, A. G., 1964, The Löfer cyclothems of the alpine Triassic; *in*, Symposium on Cyclic Sedimentation, Merriam, D. F., ed.: Kansas Geological Survey, Bulletin 169, p. 107–149

_____, 1988, Cyclostratigraphy; *in*, Global Sedimentary

Geology Program—Cretaceous Resources, Events, Rhythms, Beaudoin, B., and Ginsburg, R. N., eds.: NATO International Exchange Program, Digne, France, 286 p.

Ginsburg, R. N., 1971, Landward movement of carbonate mud—new model for regressive cycles in carbonates (abs.): American Association of Petroleum Geologists Bulletin, v. 55, p. 340

Goldhammer, R. K., Dunn, P. A., and Hardie, L. A., 1987, High-frequency glacio-eustatic sea-level oscillations with Milankovitch characteristics recorded in the Middle Triassic platform carbonate in northern Italy: American Journal of Science, v. 287, p. 853–892

_____, 1990, Depositional cycles, composite sea-level changes, cycle stacking patterns, and the hierarchy of stratigraphic forcing—examples from Alpine Triassic platform carbonates: Geological Society of America Bulletin, v. 102, p. 535–562

Grotzinger, J. P., 1986, Cyclicity and paleoenvironmental dynamics, Rocknest platform, northwest Canada: Geological Society of America Bulletin, v. 97, p. 1,208–1,231

Haq, B. U., Hardenbol, J., and Vail, P. R., 1988, Mesozoic and Cenozoic chronostratigraphy and eustatic cycles; *in*, Sea–Level Changes—An Integrated Approach, Wilgus, C. K., Hastings, B. S., Kendall, C. G. St. C., Posamentier, H. W., Ross, C. A., and Van Wagoner, J. C., eds.: Society of Economic Paleontologists and Mineralogists, Special Publication 42, p. 71–108

Hardie, L. A., and Shinn, E. A., 1986, Carbonate depositional environments, modern and ancient—pt. 3, tidal flats: Colorado School of Mines Quarterly, v. 81, 74 p.

Hays, J. D., Imbrie, J., and Shackleton, J. J., 1976, Variations in the earth's orbit—pacemaker of the Ice Ages: Science, v. 194, p. 1,121–1,132

Imbrie, J., Hays, J. D., Martinson, D. G., McIntyre, A., Mix, A. C., Morley, J. J., Pisias, N. G., Prell, W. L., and Shackleton, N. J., 1984, The orbital theory of Pleistocene climate; *in*, Milankovitch and Climate, Berger, A., Imbrie, J., Hays, J., Kukla, G., and Saltsman, B., eds.: Reidel, Boston, p. 269–306

James, N. P., 1984, Facies models 7—introduction to carbonate facies models: Geoscience Canada, v. 4, no. 3, p. 123–136

Jenny, J., Le Marrec, A., and Monbaron, M., 1981, Le couches rouges du Jurassique moyen du Haut Atlas central (Maroc)—correlation litho-stratigraphiques, elements de datations et cadre tectono-sedimentaire: Bulletin de la Societé Géologique de France, v. 23, p. 627–639

Jenkyns, H. C., Sarti, M., Masetti, D., and Howarth, M. K., 1985, Ammonites and stratigraphy of Lower Jurassic black shales and pelagic limestones from the Belluno trough, southern Alps: Ecologae Geologicae Helvetiae, v. 78, p. 299–311

Jossen, J. A., 1987, La plate-forme carbonatée Liasique du fond du Golfe Haut–Atlasique (Maroc)—evolution paleogéographique: 112e Congrés National des Societés Savantes, Lyon, France, IIe Colloque Geologie Africaine, p. 45–55

Kendall, C. G. St. C., and Lerche, I., 1988, The rise and fall of eustasy; *in*, Sea-level Changes—An Integrated Approach, Wilgus, C. K., Hastings, B. S., Kendall, C. G. St. C., Posamentier, H. W., Ross, C. A., and Van Wagoner, J. C., eds.: Society of Economic Paleontologists and Mineralogists, Special Publication 42, p. 3–17

Kendall, C. G. St. C., and Schlager, W., 1981, Carbonates and relative changes in sea level: Marine Geology, v. 44, p. 181–212

Kendall, C. G. St. C., and Warren, J., 1987, A review of the origin and setting of tepees and their associated facies: Sedimentology, v. 34, p. 1,007–1,027

Kenter, J. A. M., and Campbell, A. E., 1991, Sedimentation on a Jurassic carbonate flank—geometry, sediment fabric, and related depositional structures (Djebel Bou Dahar, High Atlas, Morocco): Sedimentary Geology, v. 72, p. 1–34

Koerschner, W. F., III, and Read, J. F., 1989, Field and modeling studies of Cambrian carbonate cycles, Virginia Appalachians: Journal of Sedimentary Petrology, v. 59, p. 654–687

Kominz, M. A., and Bond, G. C., 1990, A new method of testing periodicity in cyclic sediments: Earth and Planetary Science Letters, 98, p. 233–244

Lee, C. W., and Burgess, C. J., 1978, Sedimentation and tectonic controls in the Early Jurassic Central High Atlas trough: Geological Society of America Bulletin, v. 89, p. 1,199–1,204

Mattauer, M., Proust, F., and Tapponnier, P., 1972, Major strike-slip faults of late Hercynian age in Morocco: Nature, v. 237, p. 160–162

Monbaron, M., 1981, Sedimentation, tectonique synsedimentaire et magmatisme basique—l'evolution paleogeographique et structurale de l'Atlas de Beni Mellal (Maroc) au cours du Mesozoique; ses incidences sur la tectonique tertiaire: Ecologae Geologicae Helvetiae, v. 74, p. 625–638

Posamentier, H. W., and Vail, P. R., 1988, Eustatic controls on clastic deposition, II—sequence and systems tracts models; *in*, Sea–Level Changes—An Integrated Approach, Wilgus, C. K., Hastings, B. S., Kendall, C. G. St. C., Posamentier, H. W., Ross, C. A., and Van Wagoner, J. C., eds.: Society of Economic Paleontologists and Mineralogists, Special Publication 42, p. 125–154

Pratt, B. R., and James, N. P., 1986, The tidal flat island model for peritidal shallowing-upward sequences—St. George Group, western Newfoundland: Sedimentology, v. 33, p. 313–345

Read, J. F., and Goldhammer, R. K., 1988, Use of Fischer plots to define third-order sea-level curves in Ordovician peritidal cyclic carbonates, Appalachians: Geology, v. 16, p. 895–899

Read, J. F., Grotzinger, J. P., Bova, J. A., and Koerschner, W. F., 1986, Models for generation of carbonate cycles: Geology, v. 14, p. 107–110

Sarg, J. F., 1988, Carbonate sequence stratigraphy; *in*, Sea–Level Changes—An Integrated Approach, Wilgus, C. K., Hastings, B. S., Kendall, C. G. St. C., Posamentier, H. W., Ross, C. A., and Van Wagoner, J. C., eds.: Society of Economic Paleontologists and Mineralogists, Special Publication 42, p. 155–182

Schwarzacher, W. 1964, An application of statistical time-series analysis of a limestone shale sequence: Journal of Geology, v. 72, p. 195–213

_____, 1975, Sedimentation models and quantitative stratigraphy: Elsevier, New York, 382 p.

_____, 1987, The analysis and interpretation of stratification cycles: Paleoceanography, v. 2, p. 79–95

Septfontaine, M., 1986, Depositional environments and associated foraminifera (lituolids) in the middle Liassic carbonate platform of Morocco: Revue de Micropaleontologie, v. 28, p. 265–289

Shinn, E. A., 1983, Recognition and economic significance of ancient carbonate tidal flats—a comparison of modern and ancient examples; *in*, Recognition of Depositional Environments of Carbonate Rocks, Scholle, P. A., ed.: American Association of Petroleum Geologists, Memoir 33, p. 172–210

Stets, J., and Wurster, P., 1982, Atlas and Atlantic—structural

relations; *in*, Geology of the Northwest Africa Continental Margin, von Rad, U., Hinz, K, Sarnthein, M., and Seibold, E., eds.: Springer–Verlag, New York, p. 69–85

Van Wagoner, J. C., Posamentier, H. W., Mitchum, R. M., Vail, P. R., Sarg, J. F., Loutit, T. S., and Hardenbol, J., 1988, An overview of the fundamentals of sequence stratigraphy and key definitions; *in*, Sea–Level Changes—An Integrated Approach, Wilgus, C. K., Hastings, B. S., Kendall, C. G. St. C., Posamentier, H. W., Ross, C. A., and Van Wagoner, J. C., eds.: Society of Economic Paleontologists and Mineralogists, Special Publication 42, p. 39–45

Warme, J. E., 1988, Jurassic carbonate facies of the Central and Eastern High Atlas rift, Morocco; *in*, The Atlas System of Morocco, Jacobshagen, V., ed.: Lecture Notes in Earth Sciences, Springer–Verlag, New York, 499 p.

Weedon, G. P., 1986, Hemipelagic shelf sedimentation and climatic cycles—the Jurassic (Blue Lias) of south Britain: Earth and Planetary Science Letters, v. 76, p. 321–335